An ESCRT–spastin interaction promotes fission of recycling tubules from the endosome

Rachel Allison,[1,3] Jennifer H. Lumb,[1,3] Coralie Fassier,[4,5,6] James W. Connell,[1,3] Daniel Ten Martin,[4,5,6] Matthew N.J. Seaman,[2,3] Jamilé Hazan,[4,5,6] and Evan Reid[1,3]

[1]Department of Medical Genetics, [2]Department of Clinical Biochemistry, and [3]Cambridge Institute for Medical Research, University of Cambridge, Cambridge CB2 0XY, England, UK
[4]Unité Mixte de Recherche 7224, Centre National de la Recherche Scientifique, 75252 Paris, Cedex 05, France
[5]Institut National de la Santé et de la Recherche Médicale U952, 75252 Paris, Cedex 05, France
[6]Université Pierre et Marie Curie, 75252 Paris, Cedex 05, France

Mechanisms coordinating endosomal degradation and recycling are poorly understood, as are the cellular roles of microtubule (MT) severing. We show that cells lacking the MT-severing protein spastin had increased tubulation of and defective receptor sorting through endosomal tubular recycling compartments. Spastin required the ability to sever MTs and to interact with ESCRT-III (a complex controlling cargo degradation) proteins to regulate endosomal tubulation. Cells lacking IST1 (increased sodium tolerance 1), an endosomal sorting complex required for transport (ESCRT) component to which spastin binds, also had increased endosomal tubulation. Our results suggest that inclusion of IST1 into the ESCRT complex allows recruitment of spastin to promote fission of recycling tubules from the endosome. Thus, we reveal a novel cellular role for MT severing and identify a mechanism by which endosomal recycling can be coordinated with the degradative machinery. *Spastin* is mutated in the axonopathy hereditary spastic paraplegia. Zebrafish spinal motor axons depleted of spastin or IST1 also had abnormal endosomal tubulation, so we propose this phenotype is important for axonal degeneration.

Introduction

Endosomal sorting decisions control plasma membrane receptor concentrations, which in turn are critical in determining the cellular response to the extracellular environment. Key decisions occur in peripheral early endosomes, where receptors destined for recycling are sorted into tubular compartments for traffic away from the intraluminal vesicles (ILVs) of the degradative late endosomal/lysosomal compartment (Maxfield and McGraw, 2004). Endosomal tubulation is coordinated with degradation, as it predominantly occurs at the transition between the early and late endosome, but the mechanisms underlying this coordination are unknown (van Weering et al., 2012).

The formation of tubules at early sorting endosomes is important in both the recycling and endosome to Golgi pathways. In the recycling pathway, tubules traffic cargo from the peripheral sorting endosome to the plasma membrane directly or indirectly via a perinuclear endosomal compartment. The sorting of nutrient receptors, such as the transferrin (Tfn) receptor (TfnR), involves these tubules and is thought to occur via iterative geometric sorting. In this process, the high surface to volume ratio of the tubule favors bulk flow of the receptor into the tubule, and repeated rounds of tubulation achieve efficient sorting (Maxfield and McGraw, 2004). In contrast, certain receptors possessing a specific sorting signal are recycled to the plasma membrane via a less dynamic set of endosomal tubules (Lauffer et al., 2010; Temkin et al., 2011), whereas in the endosome to Golgi pathway, cargoes are sorted into tubules by the retromer complex (Seaman, 2004; Bonifacino and Hurley, 2008).

The machinery controlling formation and fission of endosomal tubules is being elucidated. Tubule formation is driven by proteins that contain BAR (Bin–Amphiphysin–Rvs) domains, banana-shaped domains that sense or induce membrane curvature

Correspondence to Evan Reid: ealr4@cam.ac.uk

Abbreviations used in this paper: BMP, bone morphogenetic protein; ESCRT, endosomal sorting complex required for transport; hpf, hour postfertilization; HSP, hereditary spastic paraplegia; ILV, intraluminal vesicle; M6PR, mannose 6-phosphate receptor; mGFP, membrane-associated GFP; MIT, MT interacting and trafficking; MO, morpholino; MT, microtubule; MVB, multivesicular body; Tfn, transferrin; TfnR, Tfn receptor; WASH, Wiskott–Aldrich syndrome protein and SCAR homologue.

© 2013 Allison et al. This article is distributed under the terms of an Attribution–Noncommercial–Share Alike–No Mirror Sites license for the first six months after the publication date (see http://www.rupress.org/terms). After six months it is available under a Creative Commons License (Attribution–Noncommercial–Share Alike 3.0 Unported license, as described at http://creativecommons.org/licenses/by-nc-sa/3.0/).

The Rockefeller University Press $30.00
J. Cell Biol. Vol. 202 No. 3 527–543
www.jcb.org/cgi/doi/10.1083/jcb.201211045

(Frost et al., 2009). These proteins include SNX1 (sorting nexin 1) at several pathways, including the endosome to Golgi pathway, and SNX4 at the recycling pathway (Carlton et al., 2004; Traer et al., 2007; Nisar et al., 2010). Tubule extension and fission from the endosome is believed to be accomplished by the combined action of an actin-dependent pushing force, a microtubule (MT)-dependent pulling force generated by dynein motors, and membrane scission by dynamin. The actin network implicated in this process is generated by the Wiskott–Aldrich syndrome protein and SCAR homologue (WASH) complex, which contains strumpellin, a protein involved in hereditary spastic paraplegia (HSP; Derivery et al., 2009; Gomez and Billadeau, 2009). In addition, domains that induce membrane curvature by insertion of shallow hydrophobic wedges into one leaflet of the membrane bilayer can directly promote tubule fission (Boucrot et al., 2012). Loss of key proteins involved in tubule formation can result in mistrafficking of receptors, including the TfnR, that are normally sorted via the relevant tubules (Carlton et al., 2004; Traer et al., 2007).

Inward budding of endosomal membrane to form the ILVs of the late endosome/multivesicular body (MVB) exposes receptor cargo to lysosomal enzymes (Piper and Katzmann, 2007). Sorting of cargoes into, together with formation of, the internal vesicles is accomplished by the endosomal sorting complex required for transport (ESCRT)–0, –I, –II, and –III complexes (Babst et al., 2002a,b; Hanson et al., 2009; Hurley, 2010; Henne et al., 2011). The ESCRT-III complex carries out the final membrane scission step in this process, in which the internal vesicle is released from the limiting membrane (Wollert et al., 2009; Carlton, 2010; Henne et al., 2012). In mammals, ESCRT-III comprises 11 related charged MVB proteins and IST1 (increased sodium tolerance 1), a divergent charged MVB protein that is also able to bind ESCRT-I (Bajorek et al., 2009a). The endosomal role of mammalian IST1 is not clear, as it is dispensable for sorting of cargo to the degradative compartment (Agromayor et al., 2009). Cytosolic ESCRT-III proteins, including IST1, are monomeric and autoinhibited, being activated by a conformational change that enables incorporation into the ESCRT complex and assembly at membrane (Zamborlini et al., 2006; Shim et al., 2007; Bajorek et al., 2009b). This conformational change also allows recruitment of accessory proteins to the complex, as it exposes C-terminal sequences termed MT-interacting and -trafficking (MIT) domain–interacting motifs, which bind to MIT domains. MIT domain–containing proteins include the MT-severing ATPase spastin and VPS4 (vacuolar protein sorting 4), an ATPase that catalyzes removal of the ESCRT-III complex from endosomes (Obita et al., 2007; Stuchell-Brereton et al., 2007; Hurley and Yang, 2008; Yang et al., 2008). The MIT domain of spastin binds only to CHMP1B and IST1 among the ESCRT-III proteins (Reid et al., 2005; Agromayor et al., 2009; Renvoisé et al., 2010).

Mutations in the *spastin* gene cause autosomal dominant HSP, in which there is progressive axonal degeneration of the longest axons of the corticospinal tracts. Functional analysis of spastin is therefore important in elucidating cell biological processes critical for axonal health, as well as in understanding the cellular roles of MT severing, in which internal breaks are made in MTs (Hazan et al., 1999; Blackstone et al., 2011; Lumb et al., 2012). Spastin has two main isoforms, a 616–amino acid full-length form (M1 spastin) and a form (M87 spastin) that lacks the N-terminal 86 amino acids of the full-length protein (Claudiani et al., 2005). Both isoforms are ubiquitously expressed, although in all cell types M87 spastin is much more abundant than M1 spastin. To accomplish MT severing, these spastin monomers must hexamerize and hydrolyze ATP (Roll-Mecak and Vale, 2008; Lumb et al., 2012). The M1 unique sequence of spastin contains a hairpin membrane domain that is believed to act as a hydrophobic wedge by inserting into one leaflet of the lipid bilayer (Park et al., 2010). At steady-state, M1 spastin predominantly localizes to the ER, where it is involved, with several other hairpin loop domain proteins implicated in HSP, in ER morphogenesis (Sanderson et al., 2006; Connell et al., 2009; Hu et al., 2009; Park et al., 2010; Montenegro et al., 2012). The function of MT severing in this process is unknown. Some M1 spastin may also transit endosomes (Connell et al., 2009). In contrast, M87 spastin exists in a cytosolic pool that can be recruited to endosomes or to the cytokinetic midbody in an MIT domain–dependent manner (Connell et al., 2009). At the midbody, membrane scission by ESCRT-III is coordinated with a spastin-mediated MT breakage event required to complete abscission (Yang et al., 2008; Connell et al., 2009; Guizetti et al., 2011). However, the function of spastin at endosomes is unknown.

Here, we show that cells lacking spastin have increased tubulation of early endosomal compartments and defective endosomal sorting of recycling cargo through these compartments and away from degradation, consistent with a defect in tubule fission. This phenotype was rescued by both M1 and M87 spastin but not by forms of spastin unable to sever MTs or bind to CHMP1B and IST1. Because cells lacking IST1 also had increased endosomal tubulation and defective sorting of recycling cargo, our results suggest a model in which inclusion of IST1 into the ESCRT complex triggers recruitment of spastin to promote fission of recycling tubules from the endosome. Thus, in addition to identifying novel endosomal functions of spastin and IST1, we elucidate a mechanism by which endosomal recycling can be coordinated with the degradative machinery. As we found that zebrafish spinal motor axon growth cones depleted of spastin or IST1 also had increased endosomal tubulation, we propose that this phenotype is directly linked to the axonal degeneration of HSP.

Results

Spastin regulates tubulation of early endosomal compartments

Because spastin participates in membrane modeling events at the ER and midbody, we hypothesized that endosomal spastin might also be involved in membrane modeling. Spastin depletion does not affect EGF receptor degradation and so is unlikely to influence ILV formation (Connell et al., 2009). We therefore examined the effect of spastin depletion on endosomal tubulation, analyzing endogenous SNX1 and epitope-tagged SNX4 (Carlton et al., 2004; Traer et al., 2007). In HeLa cells, depletion of all spastin isoforms using an siRNA pool caused an increase

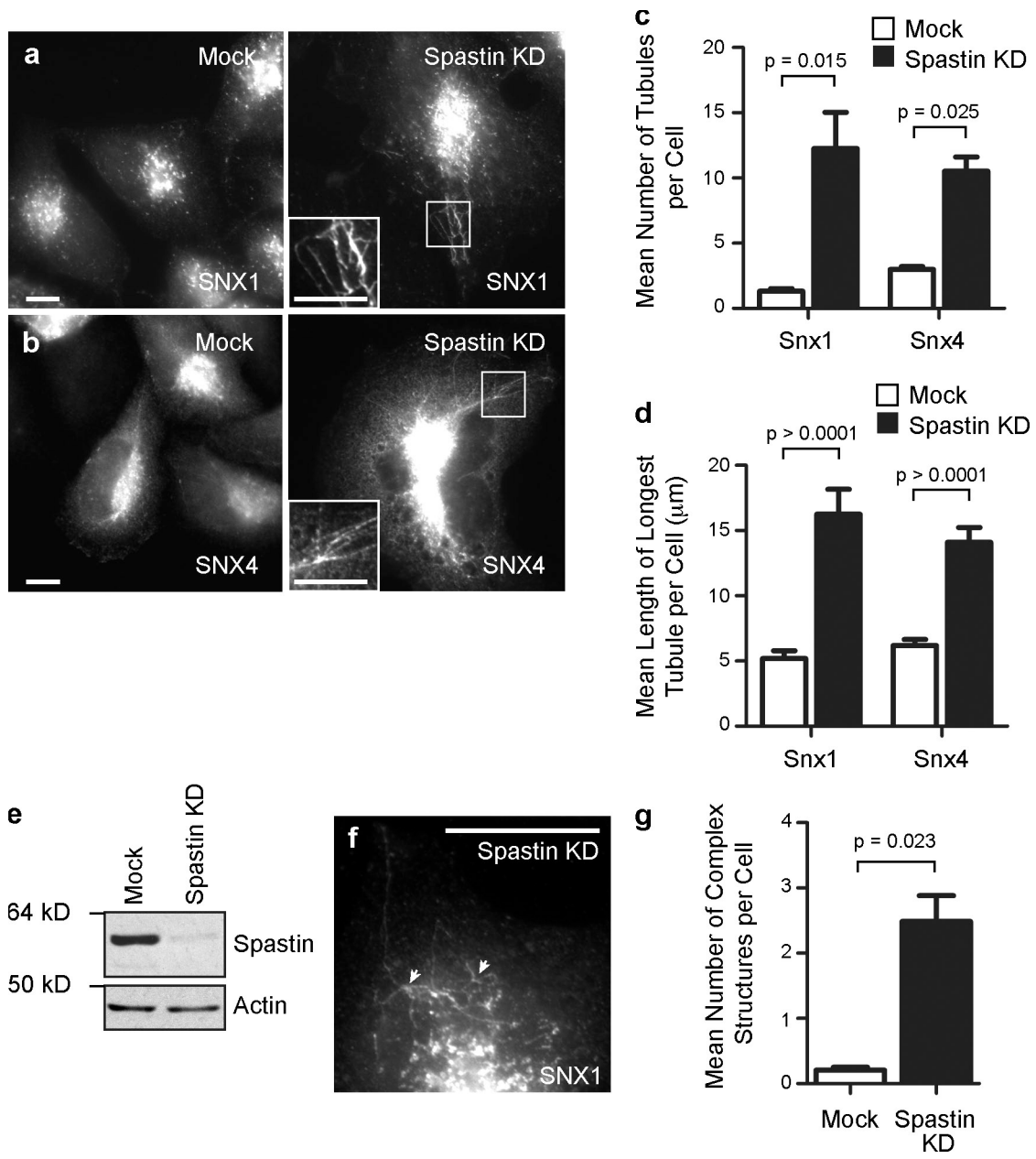

Figure 1. **Spastin regulates endosomal tubulation.** (a and b) HeLa cells were subject to mock transfection or transfection with a spastin siRNA pool (spastin knockdown [KD]) and labeled versus endogenous SNX1 (a) or transfected SNX4-mCherry (b). The insets in a and b are magnified images of the boxed regions indicated. (c) The mean number of SNX1 and SNX4 tubules per cell was quantified (n = 5 independent experiments for SNX1, and n = 3 for SNX4, 30 cells counted per experimental condition in each experiment). (d) The length of the longest tubule per cell was measured in 30 cells, and the mean values were plotted. (e) Depletion of spastin was confirmed by immunoblotting. Note that M1 spastin is not routinely seen in immunoblots such as this, in which the exposure is optimized to show the much stronger M87 band. Actin labeling is shown to verify equal sample loading. (f) Complex structures, defined as having at least three tubules emanating from a central punctum (arrowheads), were commonly seen in spastin-depleted cells. (g) The mean number of complex structures per cell was quantified (n = 3, 30 cells counted per condition in each experiment). Bars, 10 μm. Error bars show SEMs.

in the number and length of tubules labeled with these markers (Fig. 1, a–e). A similar increase in tubulation was found using three individual siRNA oligonucleotides, indicating that the increased tubulation was not an off-target effect (Fig. S1). In addition, we saw colocalization between SNX1 and SNX4-GFP on the same tubules in spastin-depleted cells (Fig. S1). Cells lacking spastin also had an increased number of complex structures, in which three or more tubules arose from a central punctum (Fig. 1, f and g). Consistent with this, live-cell imaging showed that cells lacking spastin had a more obvious and complex network of SNX4-mCherry–positive tubules than control cells. These tubules were often static (Videos 1 and 2), but when they moved, they often did so with the SNX4 puncta to which they were connected, suggesting that fission of tubules from the endosome was defective (Video 3).

Endosomal tubulation in spastin-depleted cells requires polymerized MTs

We examined whether the endosomal tubulation seen in cells lacking spastin required intact MTs. We focused on SNX1-positive

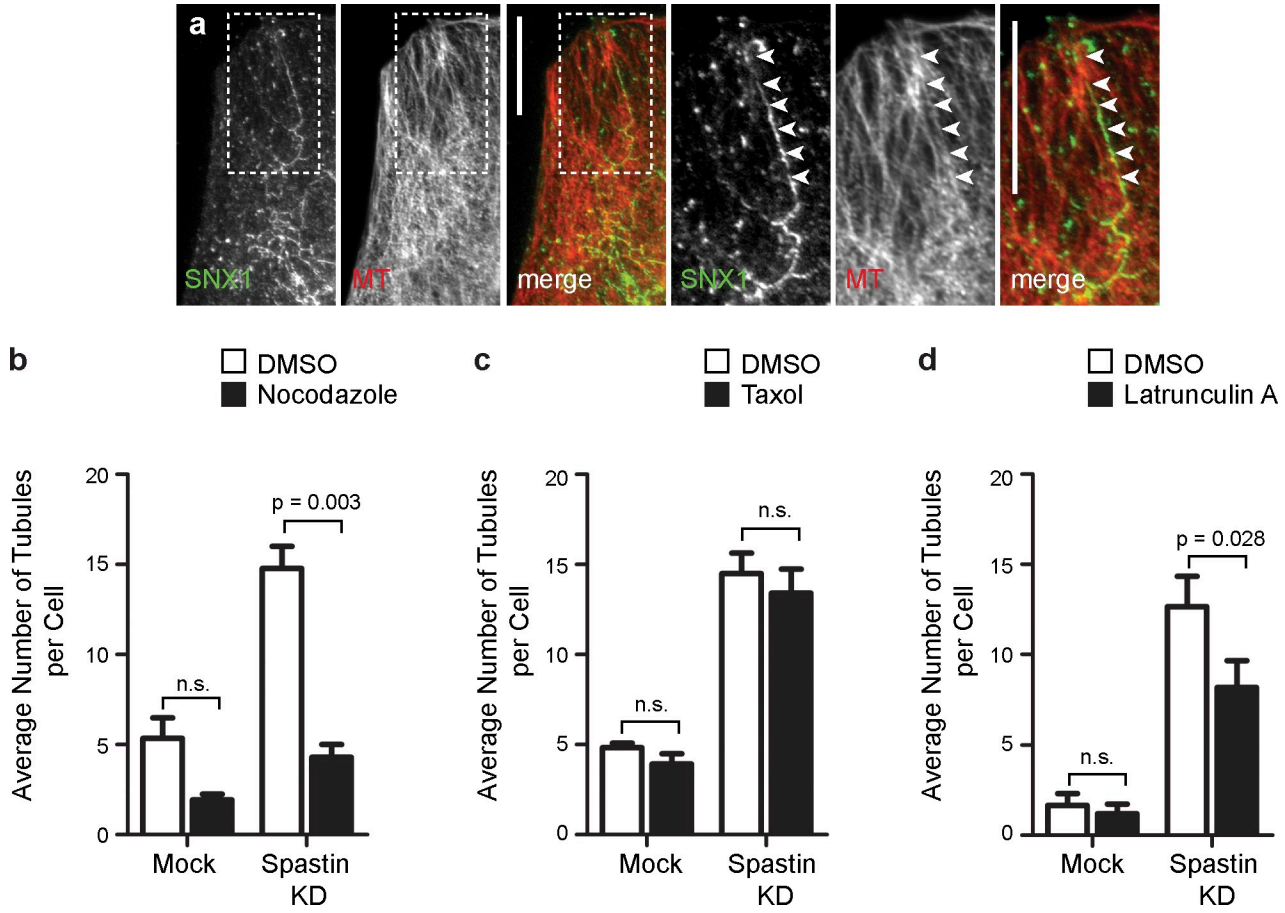

Figure 2. **Endosomal tubulation in spastin-depleted cells requires intact MTs.** (a) HeLa cells depleted of spastin by transfection with an siRNA pool were labeled with antibodies to endogenous SNX1 and α-tubulin (MT). In this and subsequent color images, the color of the lettering in the black and white images indicates the color of that image in the corresponding merged image. Arrowheads in the magnified images of the boxed areas indicate an aligned SNX1 tubule and MT. (b–d) Mock-transfected cells or cells depleted of spastin by transfection with an siRNA pool were treated with vehicle (DMSO) or the MT-depolymerizing agent nocodazole (b), the MT stabilizing agent taxol (c), or the actin-depolymerizing agent latrunculin (d), and then, the number of SNX1 tubules per cell was counted (30 cells per condition), and the mean values of three (or four for latrunculin treatment) independent experiments were plotted. Representative immunofluorescence images from these experiments are shown in Fig. S2. KD, knockdown. Bars, 10 µm. Error bars show SEMs.

tubules as a representative physiological example because we had an antibody that recognized endogenous SNX1. The SNX1 tubules induced by spastin depletion aligned along MTs (Fig. 2 a), and MT depolymerization by nocodazole significantly reduced the number of SNX1 tubules in spastin-depleted cells (Fig. 2 b and Fig. S2). We found no increase in the number of SNX1-positive tubules in HeLa cells treated with the MT-stabilizing agent taxol (Fig. 2 c and Fig. S2). We saw a small reduction in endosomal tubulation in spastin-depleted cells treated with latrunculin to prevent actin polymerization (Fig. 2 d and Fig. S2). We concluded that polymerized MTs are required for the tubulation phenotype seen in cells lacking spastin but that MT stabilization alone is insufficient to generate the phenotype.

M1 and M87 spastin isoforms regulate endosomal tubulation

We next determined which isoforms of spastin regulate endosomal tubulation. Although convincing steady-state colocalization of spastin with endogenous markers of endosomes has not been demonstrated, endogenous spastin, transiently expressed M87 spastin, and to a lesser extent transiently expressed M1 spastin are all recruited to endosomes expressing a dominant-negative form of VPS4 (VPS4-E235Q) that traps ESCRT-III and associated proteins on the endosomal membrane (Connell et al., 2009). To verify these results in a more physiological system, we generated stable cell lines expressing siRNA-resistant transcripts encoding M1 or M87 spastin. As some M87 spastin is produced by alternative translation from a second start codon (corresponding to methionine 87) in M1 spastin, the M1 construct was mutagenized (M87A) so that it would only encode the full-length isoform. Both of the stably expressed proteins were strongly recruited to endosomes (Fig. 3, a and b). We then performed siRNA rescue experiments using these cell lines and found that the endosomal tubulation phenotype seen in cells lacking endogenous spastin was rescued by either M87 or M1 spastin (Fig. 3, c–f; and Fig. S3). The tubulation phenotype was restored by additional depletion of the exogenous spastin along with endogenous spastin, confirming the specificity of the rescue by siRNA-resistant spastin (Fig. 3, c–f; and Fig. S3). We concluded that both M1 and M87 spastin are transiently and dynamically present on endosomes, and either is sufficient to rescue the endosomal tubulation phenotype seen in cells lacking spastin.

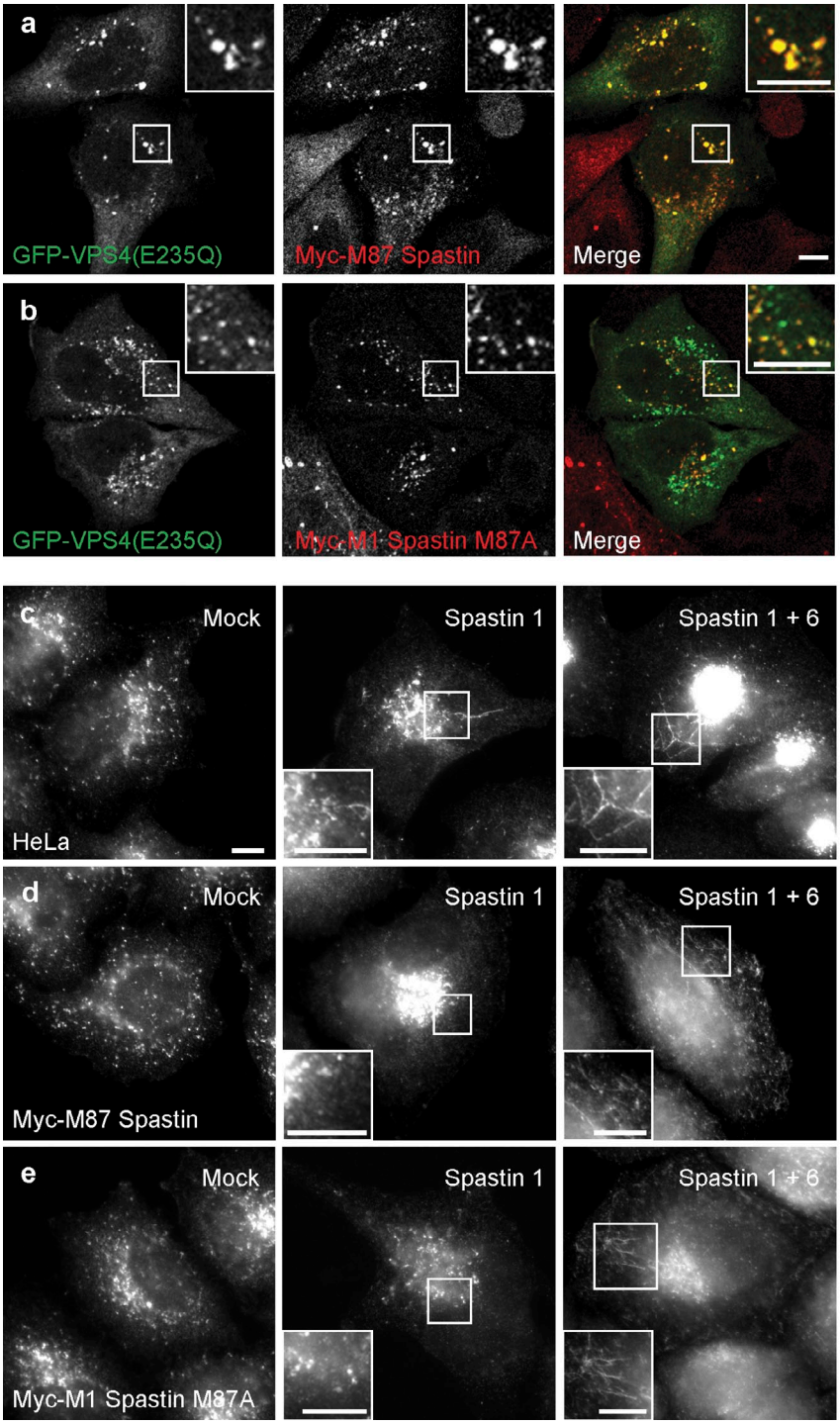

Figure 3. **M1 and M87 spastin are recruited to endosomes and regulate endosomal tubulation.** (a and b) GFP-VPS4-E235Q was transiently transfected into cell lines stably expressing myc-tagged M87 spastin (a) or myc-tagged M1 spastin M87A (b), and then, the cells were labeled with an anti-myc antibody. (c–f) HeLa cells (c), HeLa cells stably expressing myc-tagged M87 spastin (d), or HeLa cells expressing myc-tagged M1 spastinM87A (e) were subjected to mock transfection, transfected with an siRNA oligonucleotide directed against endogenous spastin (spastin 1, to which the myc-tagged transcripts were resistant), or with a combination of two siRNA oligonucleotides that together targeted endogenous and transfected spastin (spastin 1 and 6). The cells were labeled with an antibody to endogenous SNX1, and the number of SNX1 tubules per cell was counted (30 cells per condition). To control for any variation in the baseline number of tubules per cell in different cell lines, for each cell line, the mean tubule count per cell for siRNA-treated cells was normalized by subtracting the mean tubule count per cell in the corresponding mock-transfected cells. The resulting values for the mean increase in tubule number per cell in siRNA-treated cells were then plotted in f; $n = 3$ independent experiments. Cellular depletion of exogenous and/or endogenous spastin in these experiments was verified by immunofluorescence and immunoblotting (Fig. S3). Insets are magnifications of boxed regions. Bars, 10 µm. Error bars show SEMs.

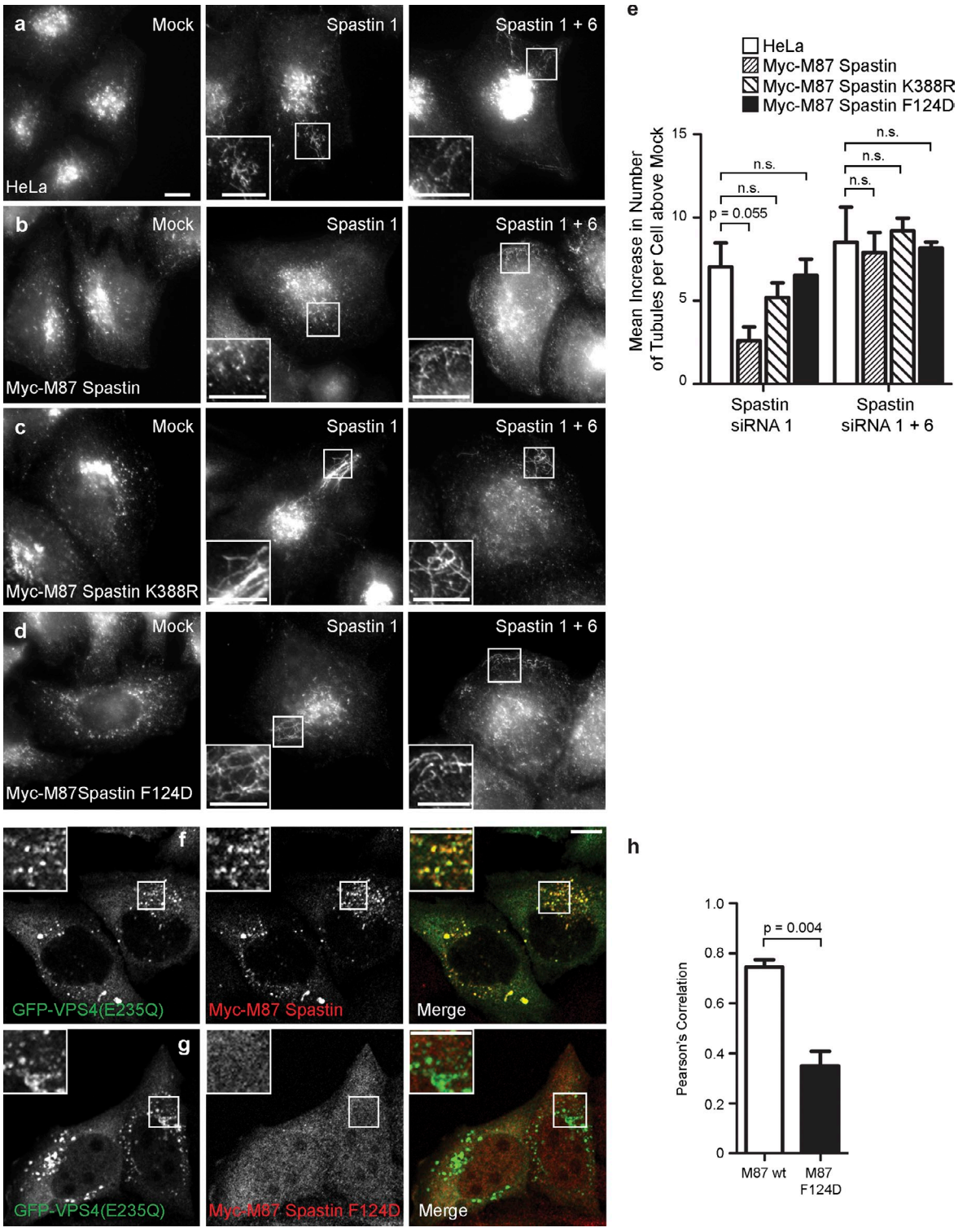

Figure 4. **ATPase activity and interaction with ESCRT-III are required for spastin to regulate endosomal tubulation.** (a–d) Wild-type HeLa cells (a), HeLa cell lines stably expressing myc-tagged M87 spastin (b), myc-tagged M87 spastinK388R (c), or myc-tagged M87 spastinF124D (d) were subjected to mock transfection or were transfected with an siRNA oligonucleotide directed against endogenous spastin (spastin 1, to which the myc-tagged transcripts were resistant) or with siRNA oligonucleotides directed against endogenous and exogenous spastin (spastin 1 and 6). Cellular depletion of exogenous and/or endogenous spastin in these experiments was verified by immunofluorescence and immunoblotting (Fig. S3). The number of SNX1 tubules per cell was counted (30 cells per condition). To control for any variation in the baseline number of tubules per cell in different cell lines, for each cell line, the mean tubule count per cell for siRNA-treated cells was normalized by subtracting the mean tubule count per cell in the corresponding mock-transfected cells. The resulting values for the mean increase in tubule number per cell in siRNA-treated cells were then plotted in e; $n = 3$ independent experiments. (f–h) GFP-tagged VPS4-E235Q was transiently transfected into HeLa cells stably expressing myc-tagged wild-type (wt) M87 spastin (f) or myc-tagged M87 spastinF124D (g), which has dramatically reduced binding to CHMP1B and IST1. The cells were labeled with anti-myc antibodies. The extent of colocalization between GFP-VPS4-E235Q and the spastin proteins was estimated by calculating the Pearson's correlation coefficient for red and green pixels in each cell, using Volocity software (h; $n = 3$ experiments, 20 cells per condition quantified in each experiment). Insets are magnifications of boxed regions. Bars, 10 µm. Error bars show SEMs.

Spastin regulates endosomal tubulation by severing MTs

As MT stabilization alone was not sufficient to cause endosomal tubulation (Fig. 2), we asked whether the ability to sever MTs was required for spastin to regulate endosomal tubulation. MT severing is catalyzed by spastin's ATPase domain. We generated a HeLa cell line stably expressing an siRNA-resistant transcript encoding M87 spastin with a disease-causing point mutation (K388R), which renders the protein ATPase defective and unable to sever MTs. Unlike cells expressing wild-type M87 spastin, we saw no rescue of the tubulation phenotype when endogenous spastin was depleted in this cell line (Fig. 4, a–c and e; and Fig. S3). We concluded that spastin requires the ability to sever MTs to regulate endosomal tubulation.

MIT–ESCRT interaction is required for spastin to regulate endosomal tubulation

We next examined whether the ability to bind CHMP1B or IST1, the two ESCRT-III proteins that interact with spastin, was required for spastin to regulate endosomal tubulation. These interactions are prevented by mutation (F124D) of a key residue in spastin's MIT domain (Yang et al., 2008; Renvoisé et al., 2010). We generated a stable cell line expressing an siRNA-resistant transcript encoding M87 spastinF124D. As expected, the presence of the F124D mutation abolished the ability of spastin to be recruited to VPS4-EQ endosomes (Fig. 4, f–h), and M87 spastinF124D was unable to rescue the increased tubulation associated with depletion of endogenous spastin (Fig. 4, d and e; and Fig. S3).

IST1 regulates endosomal tubulation

Because spastin required the ability to bind ESCRT-III to regulate endosomal tubulation, we predicted that depletion of IST1 or CHMP1B might also cause tubulation. We found no increase in endosomal tubulation in cells depleted of CHMP1B (Fig. S4). However, there was increased endosomal tubulation of the SNX1 compartment in HeLa cells depleted of IST1 by transfection with either of two different siRNA oligonucleotides (Fig. 5, a–c; and Fig. S4). This endosomal tubulation phenotype was rescued by stable expression of siRNA-resistant IST1, confirming that it is not an off-target effect (Fig. 5, d–g). In addition, the SNX1 tubules observed on IST1 depletion aligned on MTs and responded to drug treatments to depolymerize or stabilize MTs, or to depolymerize actin, in an almost identical way to those seen after spastin depletion (Fig. 5, h–k). Consistent with these results, previous immunofluorescence experiments have shown that endogenous IST1 is closely associated with SNX1 (Agromayor et al., 2009). We concluded that IST1 is the key ESCRT protein coordinating the activity of spastin in regulating endosomal tubulation.

We also examined whether IST1 or CHMP1B is required for recruitment of spastin to VPS4-EQ endosomes, by depleting each protein individually. Neither protein was necessary for this, although CHMP1B depletion caused a partial reduction in spastin recruitment (Fig. S4). The recruitment of spastin after depletion of these proteins individually is probably a result of redundancy between them, compounded by the effect of VPS4-EQ in concentrating ESCRT proteins at the endosome; for example, concentration of CHMP1B at the endosome could compensate for lack of IST1. We could not determine whether depletion of both proteins together prevented spastin's recruitment to VPS4-EQ endosomes, as it was highly toxic. Thus, these results do not exclude IST1 from playing a physiological role in recruitment of spastin to endosomes or to specific endosomal subdomains.

Spastin and IST1 are required for correct TfnR sorting

We next assessed whether the increased endosomal tubulation seen in cells lacking spastin correlated with functional effects on receptor traffic. We examined TfnR, a well-characterized receptor trafficked via the tubular recycling compartment. After endocytosis, TfnR is trafficked back to the plasma membrane via the SNX4-positive tubular compartment arising from early sorting endosomes. SNX4 depletion inhibits this traffic, probably because endosomal tubule formation is inefficient, and over repeated rounds of endocytosis and recycling this cause missorting of TfnR to the degradative compartment (Traer et al., 2007). We predicted that if depletion of spastin caused defective tubular fission, it should affect TfnR traffic in a similar fashion.

We examined TfnR concentration in cells depleted of spastin and found by immunoblotting that total cellular TfnR was reduced by >50% (Fig. 6, a and b). This reduction was partially rescued by treatment with the lysosomal inhibitor bafilomycin (Fig. 6, c and d). Consistent with this rescue by bafilomycin, immunofluorescence microscopy showed that vesicular TfnR signal remaining in cells lacking spastin was much more extensively colocalized with the late endosomal marker mannose 6-phosphate receptor (M6PR) than in wild-type cells, indicating that it had been mistrafficked to the degradative compartment (Fig. 6, e–g). In addition, we saw significant tubulation of a subset of the remaining TfnR (Fig. S5); these TfnR-positive tubules partially colocalized with SNX4-GFP and endogenous SNX1 (Fig. S5). In contrast, we saw no tubulation of M6PR. As M6PR traffics from endosomes to Golgi in a SNX1-dependent fashion (Carlton et al., 2004), this suggests that spastin depletion causes tubulation of only a subset of SNX1 pathways. In keeping with the observed effects on TfnR concentration and traffic, using a FACS-based assay, we found that cell surface TfnR was significantly reduced in spastin-depleted cells (Fig. 6 h) and that Tfn uptake was reduced by ∼50% at 20 min after incubation with fluorescently labeled Tfn (Fig. 6, i–k). In contrast, the rate of loss of cell-associated labeled Tfn after an uptake pulse, conventionally taken to represent recycling of internalized Tfn back to the cell surface, was not affected by spastin depletion. This is consistent with the loss of TfnR in cells lacking spastin being a gradual process that occurs over many rounds of endocytosis and recycling (Fig. 6, l and m). We concluded that spastin depletion inhibits traffic of TfnR away from early sorting endosomes, and instead, the receptor is missorted to the late endosomal–lysosomal degradative compartment.

We also examined TfnR traffic in cells depleted of IST1. Total cellular TfnR concentration was reduced by ∼50% on immunoblotting (Fig. 7, a and b), and this reduction was rescued by lysosomal inhibition (Fig. 7, c and d). Under immunofluorescence microscopy, the remaining TfnR became more tubular (Fig. 7 e), and the tubules partially colocalized with SNX4-GFP

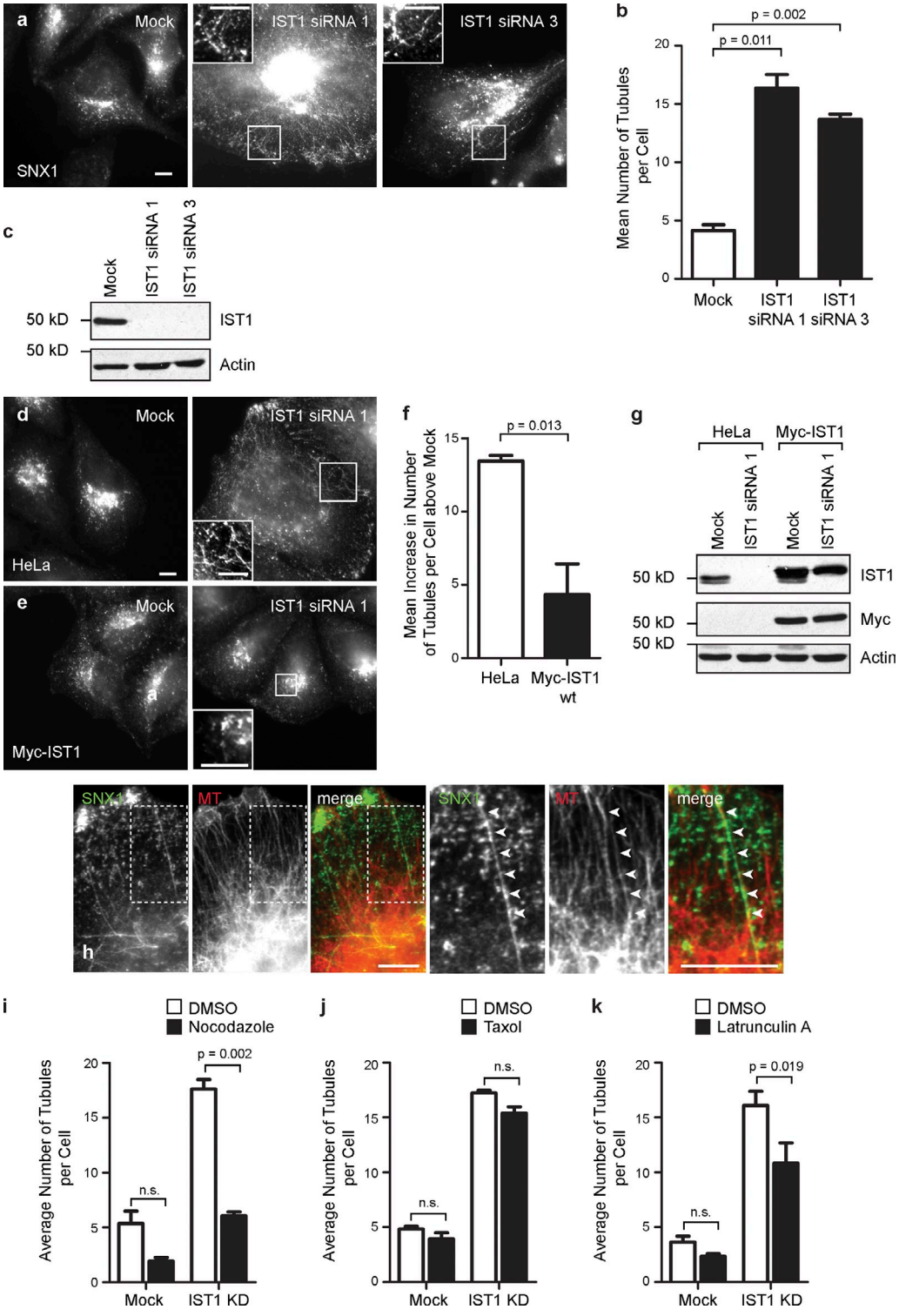

Figure 5. **IST1 regulates endosomal tubulation.** (a and b) Wild-type HeLa cells were subjected to mock transfection or transfected with either of the two IST1 siRNA oligonucleotides indicated and then labeled with SNX1. The number of SNX1 tubules per cell was counted (30 cells per condition), and the mean values of three independent experiments were plotted in b. (c) Depletion of IST1 was verified by immunoblotting. (d–g) Wild-type HeLa cells (d) or HeLa cells stably expressing myc-tagged siRNA-resistant IST1 (e) were subjected to mock transfection or were transfected with an siRNA targeting endogenous IST1. The number of SNX1 tubules per cell was counted as in a. To control for any variation in the baseline number of tubules per cell in the two cell lines, for each cell line, the mean tubule count per cell for siRNA-treated cells was normalized by subtracting the mean tubule count per cell in the corresponding mock-transfected cells. The resulting values for the mean increase in tubule number per cell in siRNA-treated cells were then plotted in f; $n = 3$ independent experiments. wt, wild type. (g) Depletion of endogenous IST1 was verified by immunoblotting. (h) HeLa cells depleted of IST1 by transfection with IST1 siRNA1 were labeled with antibodies to endogenous SNX1 and α-tubulin (MT). Arrowheads in the magnified images of the boxed areas indicate an aligned SNX1 tubule and MT. (i–k) Mock-transfected cells or cells depleted of IST1 by transfection with siRNA1 were treated with vehicle (DMSO), nocodazole (i), taxol (j), or latrunculin A (k), and then, the number of SNX1 tubules per cell was counted (30 cells per condition), and the mean values of three independent experiments were plotted. KD, knockdown. Insets are magnifications of boxed regions. Bars, 10 µm. Error bars show SEMs.

and SNX1 (Fig. S5). The remaining vesicular TfnR signal showed increased colocalization with late endosomes (Fig. 7, f–h). Finally, FACS analysis demonstrated reduced Tfn uptake (Fig. 7, i–k). These results are strikingly similar to those seen on spastin depletion and are consistent with a role for IST1 in coordinating the activity of spastin on endosomes.

Spastin and IST1 regulate endosomal tubulation in zebrafish spinal motor neuron axons

To confirm the relevance of our findings to motor neurons, we analyzed zebrafish embryos depleted of spastin or IST1 by injection with antisense morpholinos (MOs) targeting the first translation initiation site of spastin (MO^{spast}) or IST1 (MO^{IST1}). Injection of MO^{spast} resulted in a significant decrease in larval mobility, occasionally associated with a curved tail phenotype in the most severely affected (20%) MO-injected embryos (termed morphants) as previously reported (Fig. 8 a; Wood et al., 2006). Injection of MO^{IST1} also led to a reproducible decline in motility in all injected larvae and sometimes to an arched-back phenotype in the most affected morphants (25%; Fig. 8 a). Strikingly, we observed a very similar and highly reproducible phenotype of aberrant branching and truncation of spinal motor axons in both spastin and IST1 morphants at 26 h postfertilization (hpf; Fig. 8 b). This is broadly consistent with previous descriptions of spastin morphants (Wood et al., 2006). We correlated this axonal phenotype with subcellular morphological analysis of primary cultured spinal neurons derived from transgenic Tg (*Mnx1*:membrane-associated GFP [mGFP]) zebrafish. These animals selectively express GFP in spinal motor neurons, allowing their identification (Flanagan-Steet et al., 2005). Consistent with our results in HeLa cells, we found significantly enhanced tubulation of SNX1, as well as an increased number of complex tubular SNX1 structures, in the axonal growth cones of motor neurons cultured from spastin or IST1 morphant 24-hpf embryos compared with controls (Fig. 8, c–i). We concluded that spastin is required to regulate the morphology of endosomal tubules across vertebrate species and multiple cell types and including motor neuron axons.

Discussion

We have identified a novel role for spastin in regulating early endosomal tubulation and receptor sorting away from degradation and into the recycling pathway. Cells lacking spastin had increased endosomal tubulation in at least two pathways, marked by SNX1 and SNX4, which mediate sorting away from early endosomes. The increased tubulation correlated with defective sorting and increased degradation of TfnR, which normally recycles away from the degradative compartment via SNX4 tubules (Traer et al., 2007). The effects of spastin depletion on TfnR sorting were strikingly similar to those of loss of SNX4, in which the defective sorting is attributed to inefficient tubule formation (Traer et al., 2007). In contrast, in spastin-depleted cells, the combination of increased tubulation and blocked sorting strongly suggests that there is inefficient fission of endosomal tubules. Consistent with this, the tubules in spastin-depleted cells were frequently connected to a central spherical endosome, and under live-cell microscopy, connected tubules and punctate structures often moved together. Similar observations have been made in living cells lacking other proteins involved in endosomal tubule fission, such as WASH complex components or dynamin (Derivery et al., 2009; Gomez and Billadeau, 2009). We conclude that spastin promotes tubule fission.

How could spastin regulate tubule fission? Our rescue experiments showed that MT severing is critical for spastin to regulate endosomal tubulation. Each MT severing event has the potential to generate a new MT plus end, and indeed, spastin regulates the number of MT plus ends in neurite extensions or axons (Riano et al., 2009; Fassier et al., 2013). MT plus-end proteins play a role in endosomal tubulation. Depletion of the p150 glued component of the dynein–linker complex dynactin, which has a prominent localization at MT plus ends, causes increased endosomal tubulation attributed to a reduction in the dynein pulling force required for tubule fission (Wassmer et al., 2009). Consistent with this, in *Ustilago maydis*, dynein is loaded at MT plus ends, and in *Aspergillus nidulans* and mammalian cells, the plus-end protein Lis1 has a role in dynein motility of cargo (Lenz et al., 2006; Egan et al., 2012; Splinter et al., 2012). We therefore suggest that recruitment of spastin to a tubulating endosomal membrane domain provides the capacity to generate new MT plus ends that promote dynein-based traction, increasing the pulling force driving tubule fission. Interestingly, as well as M87 spastin, M1 spastin was also recruited to endosomes and could rescue the endosomal tubulation seen in cells lacking endogenous spastin. Hairpin membrane domains, as found in M1 spastin, can sense or induce high membrane curvature, and so, we suggest that incorporation of M1 spastin protomers could help appropriately localize the spastin hexamer to the highly curved membrane of the endosomal tubule. Furthermore, as domains that cause membrane curvature by shallow hydrophobic insertion may themselves cause membrane fission (Boucrot et al., 2012), this domain could directly contribute to tubule fission. It remains to be seen whether other hairpin membrane domain–containing proteins, perhaps even including those associated with HSP and which interact with M1 spastin, are also involved in this process (Park et al., 2010; Montenegro et al., 2012).

Spastin required the capacity to interact with ESCRT proteins to regulate endosomal tubulation, as F124D spastin, which can sever MTs but cannot interact with CHMP1B or IST1, was unable to rescue the endosomal tubulation seen in cells lacking endogenous spastin. Consistent with this, the effect of IST1 depletion on endosomal tubulation and TfnR trafficking was very similar to that of spastin depletion. Endosomal tubulation is coordinated with endosomal maturation, for example, SNX1 tubules are most frequent on endosomes that are at the transition point between early and late endosomes but are not present on mature late endosomes (van Weering et al., 2012). Thus, as well as identifying a novel endosomal function for IST1, our observations provide a mechanistic explanation for this coordination. They suggest a model in which the activating conformational change that occurs on recruitment of IST1 to the forming ESCRT complexes provides a spatial and temporal switch to allow interaction with spastin and to promote tubule fission and

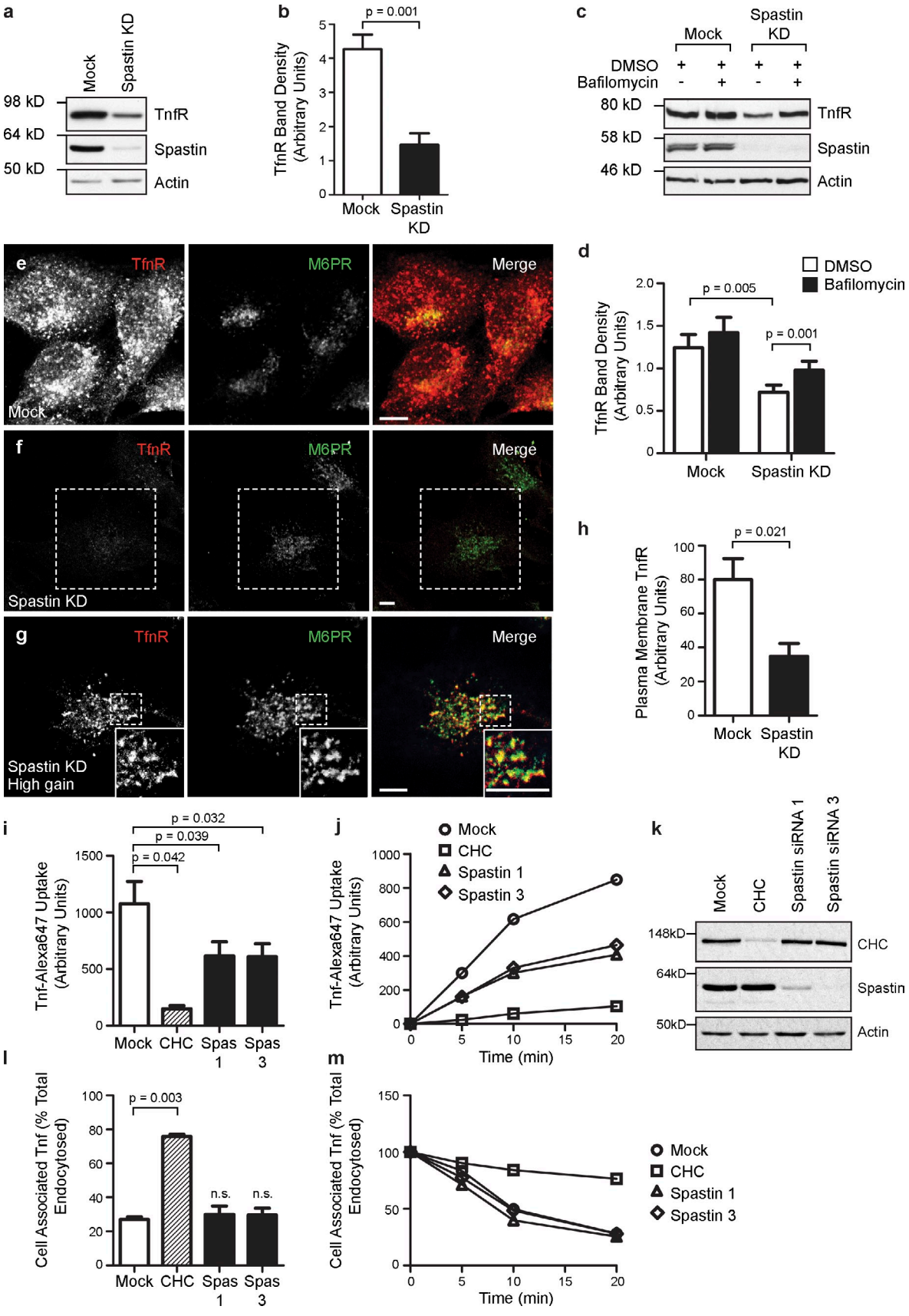

Figure 6. **Spastin is required for sorting TfnR away from degradation.** (a and b) Mock-transfected HeLa cells or HeLa cells transfected with a pool of spastin siRNA (spastin knockdown [KD]) were immunoblotted for the antibodies indicated. TfnR band density was quantified, and the mean density in three independent experiments was plotted in b. (c and d) Mock-transfected HeLa cells or HeLa cells transfected with a pool of spastin siRNA were treated

receptor recycling before the endosome becomes committed to the degradative compartment (Zamborlini et al., 2006; Shim et al., 2007; Yang et al., 2008; Bajorek et al., 2009b). As IST1 can interact with ESCRT-I as well as ESCRT-III, this recruitment could begin early in the formation of the ESCRT complexes, an idea supported by the close association seen under immunofluorescence microscopy between endogenous IST1 and SNX1 or the early endosomal marker EEA1 (Agromayor et al., 2009; Bajorek et al., 2009a).

Regulation of the activity of IST1 and spastin in endosomal tubulation would provide a means to control the balance between receptor degradation and recycling and so could provide a point of control in physiological situations in which this balance is important. Interestingly, IST1 protein concentration in yeast is nutrition sensitive. In yeast, amino acid starvation causes up-regulation of the MVB pathway and increased receptor degradation to produce amino acids for reuse. IST1 protein concentration falls during amino acid starvation, and a consequence of this is activation of the MVB pathway via a mechanism proposed to involve enhancement of VPS4 activity in recycling ESCRT-III components (Jones et al., 2012). As our results show that reduced activity of the IST1-spastin machinery also inhibits sorting of receptors away from the degradative pathway, reductions in IST1 could therefore coordinate several endosomal processes to increase amino acid production during starvation.

Increased endosomal tubulation was seen in the axonal growth cones of spinal motor neurons derived from spastin- and IST1- depleted embryos, indicating that this system regulates endosomal tubulation across vertebrate species and in the axons of a cell type relevant to HSP. As spinal motor neurons lacking spastin had axonal abnormalities in vivo and as many spastin mutations are splice site, nonsense, or frameshift mutations that result in loss of function and so are appropriately modeled by spastin depletion, we propose that the enhanced endosomal tubulation phenotype is directly related to the axonopathy of HSP. Furthermore, M87 spastin incorporating the disease-associated K388R substitution failed to rescue the endosomal tubulation phenotype in HeLa cells lacking endogenous spastin, further supporting the relevance of endosomal tubulation to the human disease. Finally, in view of the identical cellular and axonal phenotypes of spastin and IST1 depletion, we propose that *IST1* is also a strong candidate gene for HSP.

Another HSP protein, strumpellin, has a role in fission of endosomal tubules. Strumpellin is a component of the WASH complex, the actin-regulating complex required for efficient endosomal tubule fission, and cells lacking strumpellin exhibit a similar endosomal tubulation phenotype to that seen on spastin depletion (Harbour et al., 2010). More circumstantially, the HSP protein spartin binds to IST1 and so could influence the role of IST1 in endosomal tubulation (Renvoisé et al., 2010). We therefore suggest that dysregulation of endosomal tubulation could be a common pathogenic mechanism that leads to HSP by causing abnormal traffic of receptors important for axonal signaling. A strong candidate to be involved is the bone morphogenetic protein (BMP) signaling pathway. Several HSP proteins, including spastin and spartin, are inhibitors of BMP signaling, and up-regulated BMP signaling is a cause of axonal abnormalities in fly and zebrafish models of HSP (Wang et al., 2007; Tsang et al., 2009; Fassier et al., 2010). This hypothesis will be a focus of our future research.

In summary, our work identifies a new endosomal role for spastin that is relevant to motor axons, identifies a mechanism coordinating endosomal degradation and recycling via a novel function of IST1, and reveals the involvement of MT-severing machinery in membrane fission events. It will form the foundation of future work aimed at further understanding the mechanisms of endosomal sorting and tubule fission, the cellular roles of MT severing, and the molecular and cellular pathogenic mechanisms leading to HSP.

Materials and methods

Antibodies

Rabbit polyclonal anti-spastin86–340 (available from EMD Millipore) was raised against maltose binding protein fused to amino acids 86–340 of M1 spastin, rabbit polyclonal anti-M6PR was raised to GST fused to a portion of the cytoplasmic tail of rat M6PR equivalent to amino acids 2,347–2,487 of the human M6PR sequence, and rabbit polyclonal anti-SNX1 was raised against a GST-mouse SNX1 fusion protein (Reaves et al., 1996; Seaman, 2004; Connell et al., 2009). Rabbit polyclonal anti-CHMP1B was raised (Harlan Sera-Lab) against a GST-CHMP1B fusion protein that was made in house by bacterial expression of a pGEX construct containing the coding sequence of human CHMP1B. Mouse monoclonal antispastin (6C6), mouse monoclonal α-tubulin (DM1A), and rabbit polyclonal anti-actin antibodies were obtained from Sigma-Aldrich. Mouse monoclonal antimyc (4A6) was obtained from EMD Millipore. Mouse monoclonal anti-TfnR and mouse monoclonal anti-GFP (3E6) were purchased from Invitrogen. Rabbit polyclonal anti-IST1 was obtained from Proteintech Group, Inc. Rabbit polyclonal anti-EGFR (sc-03) was obtained from Santa Cruz Biotechnology, Inc. Rabbit polyclonal anti-H2b (histone H2b; ab1790) and mouse monoclonal anti-M6PR (ab2733) were purchased from Abcam. Rabbit polyclonal anti-GAPDH antibody was obtained from Cell Signaling Technology. Mouse monoclonal anti–znp-1 antibody was obtained from the

with vehicle (DMSO) or DMSO + bafilomycin and then immunoblotted versus the antibodies indicated. TfnR band density was quantified, and the mean density in eight independent experiments was plotted in d. (e–g) Confocal micrographs of HeLa cells subjected to mock transfection (e) or transfected with a spastin siRNA pool (f and g) and then labeled with the markers shown. Confocal micrograph gain settings were identical in e and f, but in g, which shows a higher magnification image of the dashed area indicated in f, gain settings were increased to reveal that the remaining TfnR signal strongly colocalized with M6PR. Note that tubular TfnR structures are not readily seen under confocal microscopy, as the tubules tend to leave the plane of section. Insets are magnified regions of the boxed areas. (h) Mock-transfected HeLa cells or HeLa cells transfected with a pool of spastin siRNA were fixed and labeled (without permeabilization) with a FITC-conjugated antibody against TfnR, and then, the cell-associated fluorescent signal was quantified by FACS analysis. The mean fluorescence values for three independent experiments were plotted. (i–k) Uptake of Alexa Fluor 647–conjugated Tfn was measured by FACS over a 20-min time course in mock-transfected HeLa cells, cells transfected with siRNA targeting clathrin heavy chain (CHC), or cells transfected with one of two siRNAs directed against spastin (spas1, spastin 1; spas3, spastin 3). Mean Tfn uptake at the 20-min time point (n = 3 experiments) is shown in i, and a representative time course experiment is shown in j. Depletion of the relevant proteins targeted by siRNA was confirmed by immunoblotting, and a representative example is shown in k. (l and m) Recycling of internalized fluorescently labeled Tfn was measured over a 20-min time course, and the mean cell-associated Tfn at the 20-min time point (n = 3 experiments) is shown in l, with a representative time course experiment shown in m. Bars, 10 µm. Error bars show SEMs.

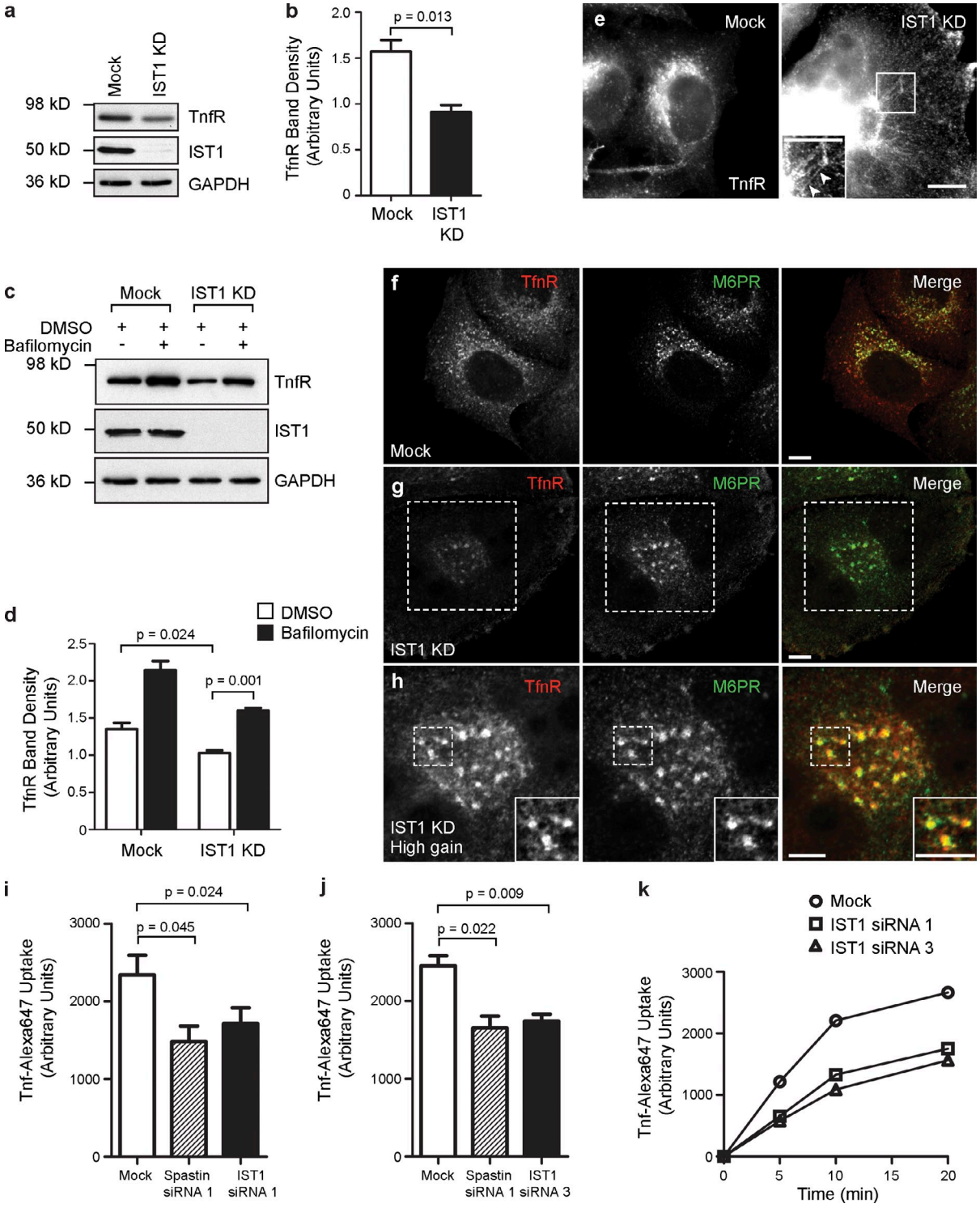

Figure 7. **Ist1 is required for sorting TfnR away from degradation.** (a and b) Mock-transfected HeLa cells or HeLa cells transfected with IST1 siRNA1 (IST1 knockdown [KD]) were immunoblotted for the antibodies indicated. TfnR band density was quantified, and the mean density in three independent experiments was plotted in b. GAPDH immunoblotting serves as a loading control. (c and d) Mock-transfected HeLa cells or HeLa cells transfected with IST1 siRNA1 were treated with vehicle (DMSO) or DMSO + bafilomycin and then immunoblotted versus the antibodies indicated. TfnR band density was quantified, and the mean density in three independent experiments was plotted in d. (e) Mock-transfected HeLa cells or HeLa cells transfected with IST1 siRNA1 were labeled for TfnR. Increased TfnR tubulation is seen in the IST1-depleted cells (see arrowheads in inset magnified region of the boxed area). The exposure settings in the IST1 knockdown image have been increased to compensate for the reduced TfnR levels in these cells. (f–h) Confocal micrographs of HeLa cells subjected to mock transfection (f) or transfected with IST1 siRNA1 (g and h) and then labeled with the markers shown. Confocal micrograph gain settings were identical in f and g, but in h, which shows higher magnification images of the dashed areas indicated in g, gain settings were increased to reveal that the remaining TfnR signal strongly colocalized with M6PR. Insets are magnified areas of the boxed regions. (i–k) Uptake of Alexa Fluor Tfn 647 was measured by FACS over a 20-min time course in mock-transfected HeLa cells, cells transfected with spastin siRNA1 (as a positive control), and IST1 siRNA1 (i) or IST1 siRNA3 (j). Mean Tfn uptake at the 20-min time point is shown (n = 3 experiments plotted for each histogram). A representative time course experiment is shown in k. Bars, 10 µm. Error bars show SEMs.

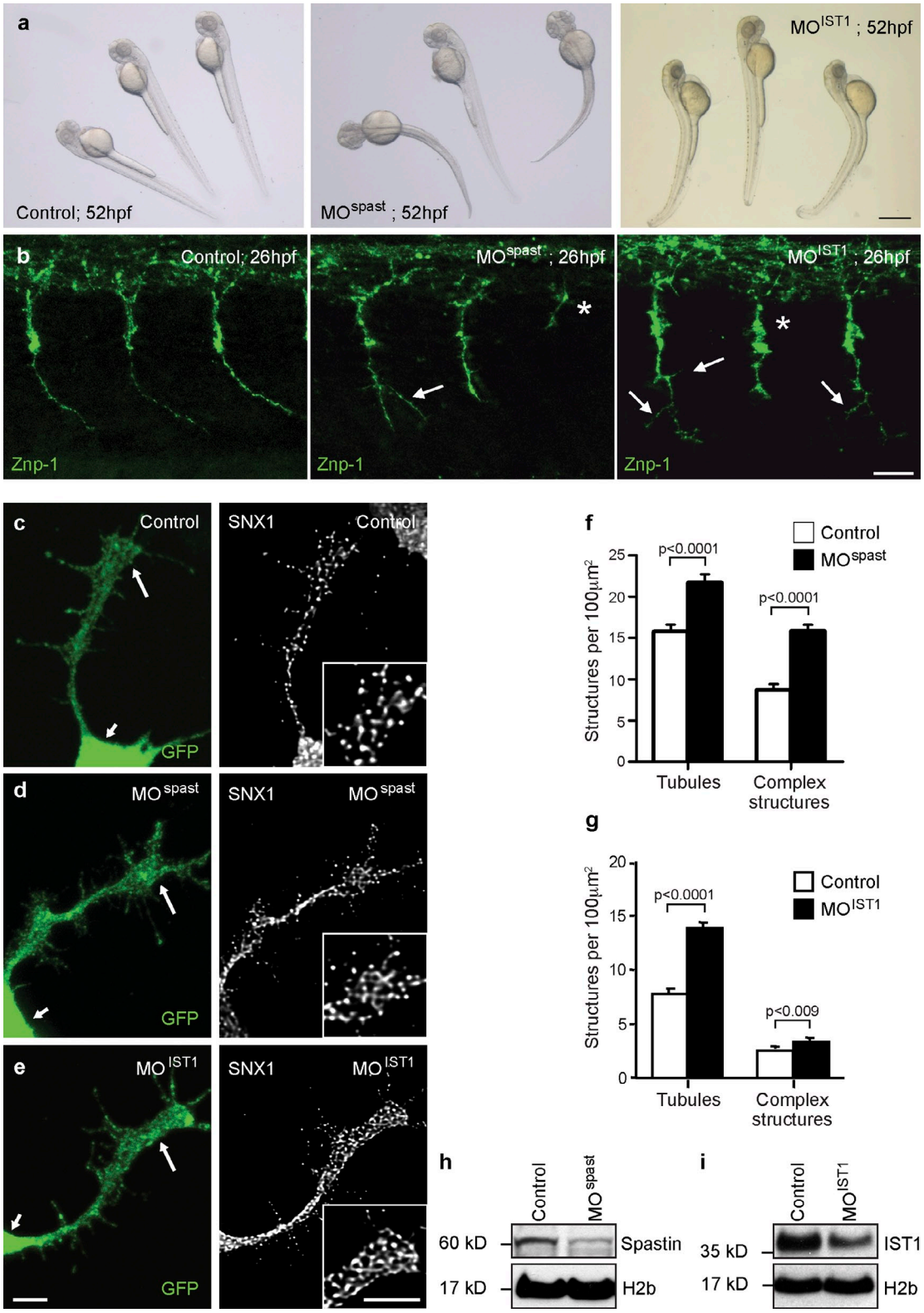

Figure 8. **Spastin regulates endosomal tubulation in spinal motor axonal growth cones.** (a) Gross phenotype of 52-hpf control, spastin morphant (MO^{spast}), and IST1 morphant (MO^{IST1}) zebrafish larvae. Bar, 500 μm. (b) Whole-mount immunohistochemistry of 26-hpf zebrafish control, MO^{spast}, and MO^{IST1} embryos labeled with the motor neuron marker synaptotagmin 2 (znp-1). Images are lateral views of the trunk; anterior is to the left. Axonal stumps (asterisks) and abnormal branching (arrows) of spinal motor neuron axons were observed in all spastin and IST1 morphants. Bar, 25 μm. (c–i) Spinal neurons were cultured from control (c), spastin morphant (d), and IST1 morphant (e) 24-hpf Tg(*Mnx1*:mGFP) embryos, in which GFP is selectively expressed in motor neurons. Cultured neurons were labeled with SNX1 and GFP antibodies, and the mean number of SNX1-positive tubules and complex tubular structures per 100-μm^2 region of each motor axon growth cone (large arrows in GFP-labeled images and inset boxes in SNX1-labeled images; small arrows indicate the cell body) was calculated by counting ~30 cells per condition. Bars, 5 μm. (f and g) The mean values obtained in three (f) or five (g) independent experiments were plotted. (h and i) In these experiments, spastin and IST1 depletion was verified by immunoblotting. Anti–histone H2b immunoblotting is shown to verify equal protein loading. Error bars show SEMs.

Zebrafish International Resource Center, University of Oregon. Rabbit polyclonal anti–clathrin heavy chain was a gift from S. Robinson (University of Cambridge, Cambridge, England, UK). Alexa Fluor 568 phalloidin was purchased from Invitrogen. Peroxidase-conjugated secondary antibodies for Western blotting were obtained from Sigma-Aldrich. Alexa Fluor 488– and 568–labeled secondary antibodies for immunofluorescence were obtained from Molecular Probes.

Constructs and generation of stable cell lines

pLXIN-myc-spastin constructs were generated by cloning M87 or M1 spastin into the pIRESneo2 vector (NheI–BamHI; Takara Bio Inc.) followed by insertion of a myc tag (EcoRV–NheI), and then, myc-spastin was further cloned into the pLXIN vector (SalI–BamHI; Takara Bio Inc.). Constructs were made resistant to spastin siRNA1 and 3 by introducing two mutations into each of the relevant sequences by site-directed mutagenesis. pLXIN-myc-M87-spastin-K388R and -F124D mutants were then generated by site-directed mutagenesis. Codon-optimized IST1 isoform 1 (UniProt accession no. P53990) was synthesized by GenScript. A 5′ myc tag was added by insertion of IST1 into pIRESneo2-myc (NheI–BamHI). Codon optimization of the IST1 sequence rendered it resistant to both IST1 siRNA1 and 3. Stable cell lines were generated by retroviral transfection of HeLaM cells. The GFP-VPS4-E235Q construct was a gift from P. Whitley (University of Bath, Bath, England, UK), and the SNX4-mCherry and SNX4-GFP constructs were gifts from P. Cullen (University of Bristol, Bristol, England, UK).

Cell culture and transfection

HeLaM cells were maintained as previously described (Connell et al., 2009). HeLaM cells stably expressing spastin or IST1 constructs were additionally cultured in the presence of 500 µg/ml Geneticin (Invitrogen).

In DNA transfections, HeLaM cells were transfected using the transfection kit (HeLaMONSTER; Mirus Bio LLC) following the manufacturer's protocol and incubated with transfection reagents for 24 h. For siRNA transfection, cells were transfected with the relevant siRNAs, using transfection reagent (Oligofectamine; Invitrogen), according to a 5-d protocol modified from Motley et al. (2003). In brief, HeLaM cells were plated into a well of a 6-well plate and transfected after 24 h. Cells were harvested 96 h later. Where cells were additionally transfected with a DNA construct during the knockdown, the DNA transfection was carried 72 h after siRNA transfection, and the cells were harvested 24 h later. The efficiency of siRNA knockdown was verified by immunoblotting cell lysates and/or by immunofluorescent microscopy of fixed cells, with an antibody against the relevant protein. The following siRNA sequences and concentrations were used: spastin (used at 5 nM) siRNA1, 5′-GAACUUCAACCUUCUAUAA-3′ (D-014070-01; Thermo Fisher Scientific), siRNA3, 5′-UAUAAGUGCUGCAAGUUUA-3′ (D-014070-03; Thermo Fisher Scientific), and siRNA6, 5′-UGUGGACAAUGGAACAGCUGUUAUU-3′; IST1 (used at 25 nM) siRNA1, 5′-CCAAGUAUAGCAAGGAAUA-3′ (D-020977-01; Thermo Fisher Scientific), and siRNA3, 5′-GCAAAUACGCCUUUCUCAU-3′ (D-020977-03; Thermo Fisher Scientific); and CHMP1B (used at 10 nM) siRNA1, 5′-GAAGAUUUCUGCUUUGAUGUU-3′ (D-004698-01; Thermo Fisher Scientific), siRNA6, 5′-GUCGAUGGCUGGUGUGGUU-3′ (J-004698-06; Thermo Fisher Scientific), and siRNA7, 5′-CCUUCGGGAUCAAGUGUGA-3′ (J-004698-07; Thermo Fisher Scientific).

Two other CHMP1B oligonucleotides, corresponding to Thermo Fisher Scientific catalog numbers J-004698-05 and J-004698-08 were also used; however, these were found to have significant off-target effects on the actin cytoskeleton and so excluded from further analysis. Clathrin heavy chain (catalog reference L-004001-01), an ON-TARGETplus siRNA SMARTpool (Thermo Fisher Scientific), was used at a concentration of 5 nM.

Immunofluorescence microscopy of HeLa cells

Cells were fixed at room temperature in 3.8% (vol/vol) formaldehyde in PBS and permeabilized in PBS containing 0.1% (vol/vol) Triton X-100 (Sigma-Aldrich) or, for MT labeling, were fixed and permeabilized in ice-cold methanol for 4 min. Coverslips were washed with PBS, blocked for 30 min in PBS with 10% FCS, and then labeled for 1 h each with primary and secondary antibodies diluted in PBS with 10% FCS as previously described (Connell et al., 2009). Coverslips were washed with PBS and distilled water and then mounted in ProLong Gold antifade reagent with DAPI (Invitrogen). Slides were analyzed at room temperature with a confocal microscope (63×/1.4 NA oil immersion objective; LSM 710 Meta; Carl Zeiss) with ZEN analysis software (Carl Zeiss) or using a light microscope (Axioplan [Carl Zeiss]; Plan Apochromat 63×/1.4 NA oil immersion objective [Carl Zeiss] with a digital camera [C10600; Hamamatsu Photonics]) and SimplePCI software (HCImage). Images were subsequently processed using Photoshop and Illustrator (Adobe) or ImageJ (National Institutes of Health) software. Volocity software (PerkinElmer) was used to quantify colocalization of immunofluorescence signals in 20 cells per experimental condition.

Tubulation counts on HeLa cells

Cells labeled with the appropriate marker were processed for immunofluorescence microscopy as described (see previous paragraph) and imaged at room temperature with the aforementioned light microscope (Axioplan) under a 63×/1.4 NA oil immersion objective. For each experimental condition, images of 30 cells were recorded. The images were then randomized, and the number of tubules per cell, up to a maximum of 20 tubules, was counted blind to the experimental condition. Tubules were defined as linear structures with a length >2 µm. In experiments involving cytoskeletal manipulation, before fixation, cells were incubated at 37°C with 10 µM taxol (in DMSO for 100 min), 0.4 mg/ml nocodazole (in DMSO diluted to a final concentration of 2 µg/ml for 1 h), 1 mg/ml latrunculin A (in DMSO diluted to a final concentration of 0.4 µg/ml for 45 min), or DMSO vehicle. The actin cytoskeleton was visualized with postfixation phalloidin staining (1:40).

Live-cell microscopy

Images were captured at 37°C using an inverted microscope (Axio Observer.Z1; Carl Zeiss) with a Plan Apochromat 63×/1.40 NA differential interference contrast oil objective and a camera (AxioCam MR3; Carl Zeiss) equipped with a spinning-disc module. Frames were recorded every 2 s for a maximum of 2 min. A multiple wavelength laser module was used to visualize red fluorescence, and images were processed using AxioVision software (Carl Zeiss).

TfnR and Tfn uptake and recycling assays

Total cell TnfR levels were measured with and without bafilomycin A1 treatment. Adherent HeLa cells were transfected with siRNA for 72 h. For the final 18 h, cells were incubated with 100 µM bafilomycin A1 (in DMSO diluted to a final concentration of 1 µM; Sigma-Aldrich) or DMSO vehicle and then washed and harvested in cell lysis buffer (300 mM NaCl, 50 mM Tris, pH 8.0, 5 mM EDTA, pH 8.0, and 1% [vol/vol] Triton X-100). Samples were analyzed by Western blot analysis, and bands were quantified using ImageJ software. Band intensity values were normalized against actin or GAPDH band intensity to control for loading variations.

Cell surface TnfR levels were measured as follows. Adherent HeLa cells were transfected with siRNA for 72 h and then trypsinized, resuspended in Opti-MEM, and incubated on ice with FITC-CD71 (1:5; BD) for 30 min. Cells were washed and then fixed in a solution of 3.8% formaldehyde in PBS and analyzed using a FACS machine (FACSCalibur; BD).

Tfn uptake and recycling assays were performed as previously described (Peden et al., 2004). In brief, adherent HeLa cells were transfected with siRNA for 72 h and then trypsinized, resuspended in Opti-MEM, and incubated on ice with Alexa Fluor Tfn-647 (Invitrogen). For the uptake assay, cell aliquots were then incubated at 37°C for 0, 5, 10, or 20 min before fixation. For the recycling assay, incubation of cells for 20 min at 37°C to internalize Tfn was followed by the addition of unlabeled Tfn to stimulate recycling of fluorescent Tfn to the cell surface, and cells were then incubated and fixed at time points ≤20 min. Cells were fixed in a solution of 3.8% formaldehyde in PBS and analyzed using a FACS machine (FACSCalibur).

Zebrafish maintenance

Zebrafish embryos were obtained from natural spawning of AB wild-type and transgenic Tg(*Mnx1*:mGFP) (a transgenic line in which the expression of GFP is regulated by genomic elements from the zebrafish motor neuron–expressed hb9 gene) lines (Flanagan-Steet et al., 2005). All embryos were maintained in E3 medium (5 mM NaCl, 0.17 mM KCl, 0.33 mM $CaCl_2$, 0.33 mM $MgSO_4$, and 0.00001% [wt/vol] methylene blue) at 28°C and staged by hpf as well as gross morphology according to Kimmel et al. (1995). To prevent pigment formation, 0.2 mM 1-phenyl-2-thiourea (Sigma-Aldrich) was added to E3 medium after the prim-5 stage.

MO injections and Western blot

MO oligonucleotide against *spastin* (MO^{spast}, 5′-ATTCATTCACCCTTCTCGGGCTCTC-3′) and *IST1* (MO^{IST1}, 5′-ATTTGAACCCTCCACCCAGCATGAT-3′) translation initiation sites were designed by Gene Tools. MO^{spast} and MO^{IST1} were diluted in deionized water and injected at 0.6 and 1.2 pmol/embryo, respectively, at two-cell stage. The knockdown efficiency was assessed by Western blot analysis using 20 µg of total protein extract from 24-hpf control and MO^{spast} embryos or 42-hpf control and MO^{IST1} embryos prepared in SDS sample buffer (0.5 µl per embryo; 1 M Tris-HCl, pH 6.8, 10% glycerol, 5% β-mercaptoethanol, and 3.5% SDS) complemented with

a cocktail of protease inhibitors (Roche) and 1 mM PMSF. Anti-spastin86–340, anti-IST1, and anti-Hb2 (as loading control) antibodies were used in these analyses.

In toto immunohistochemistry

Whole-mount immunohistochemistry experiments were performed on 26-hpf control and MO^{spast}- and MO^{IST1}-injected embryos. Embryos were fixed in 4% PFA for 2 h at room temperature, washed four times with PB-T1% (1% Triton X-100 in PBS), permeabilized in a 0.25% trypsin solution (at 25°C) for 2 min, blocked for 2 h in PB-T1% supplemented with 10% normal goat serum, and subsequently incubated overnight with the znp-1 antibody. After several washes in PB-T1%, embryos were incubated overnight at 4°C with an Alexa Fluor 488 goat anti–mouse (Molecular Probes). Images were acquired at room temperature using a fluorescent microscope equipped with an ApoTome module (20×/0.5 NA air objective; Axiovert 200M; Carl Zeiss) and processed using Photoshop software.

Primary culture of zebrafish spinal neurons and immunocytochemistry

Primary cultures of zebrafish spinal neurons were prepared from 24-hpf embryos as previously described (Fassier et al., 2010). In brief, spinal cords of dechorionated control and MO^{spast}- and MO^{IST1}-injected embryos were isolated by removing the yolk and the head, incubated in a Custom ATV solution (mM: 0.6 EDTA, 5.5 glucose, 5.4 KCl, 136.8 NaCl, and 5.5 Na_2CO_3) supplemented with 0.25% trypsin for 20 min at 27°C and mechanically dissociated with a drawn-out Pasteur pipette in culture medium (50% L-15 medium [Leibovitz's], 49% 10-fold diluted Ringer [mM: 115 NaCl, 2.6 KCl, 2 $CaCl_2$, and 10 Hepes, pH 7.6], 1% fetal bovine serum, and 1% penicillin/streptomycin). Cells were plated onto poly-D-ornithine/laminin-coated dishes at a density of seven spinal cords per 35-mm dish and maintained at room temperature for 8 h after plating. Zebrafish-cultured spinal neurons were fixed in 4% PFA/4% sucrose for 12 min at room temperature, permeabilized with 0.1% Triton X-100 in PBS for 8 min, blocked for an hour at room temperature in PBS supplemented with 3% BSA and 5% normal goat serum, and incubated with anti-SNX1 and anti-GFP antibodies overnight at 4°C. Cells were subsequently washed four times with PBS, incubated for an hour at room temperature with the appropriate secondary antibodies, and washed again in PBS. Images were acquired at room temperature using a confocal laser-scanning microscope (TCS SP5 Acousto-Optical Beam Splitter; Leica) and a 1.4 NA objective (oil immersion, 63×; Leica) with the pixel size set to 60 nm and a z step of 130 nm. Confocal images of SNX1 staining were deconvoluted with the Huygens 3.6 software (Scientific Volume Imaging) using a theoretical point spread function and the classical maximum likelihood estimation algorithm and adjusted for brightness and contrast with Photoshop software. The number of endosomal tubules and endosomal complex structures was counted in ∼30 control and morphant growth cones per experiment in three (MO^{spast}) or five (MO^{IST1}) independent analyses and normalized according to the growth cone area.

Statistical analysis

For experiments on HeLa cell lines, differences from at least three independent experiments examining (a) the mean number of tubules, (b) the number of complex structures, or (c) mean fluorescence as detected by FACS analysis were compared by paired (when comparing within the same cell line) or unpaired (when comparing between different cell lines) two-tailed Student's *t* tests, using Prism 5.01 for Windows (GraphPad Software) statistical software. Tubule length analysis was performed by comparing the length of the longest tubule in 30 cells from each experimental condition, using a two-tailed paired Student's *t* test.

For the zebrafish experiments, statistical analysis of differences in mean tubule or complex structure counts was performed using the Student's unpaired *t* test (StatView software; SAS Institute, Inc.). Error bars in all histograms represent SEM.

Online supplemental material

Fig. S1 shows increased endosomal tubulation in HeLa cells depleted of spastin using three separate siRNA oligonucleotides and colocalization of SNX1 and SNX4 on tubules in cell lacking spastin. Fig. S2 shows the effect of cytoskeleton-modifying drugs on endosomal tubulation in HeLa cells depleted of spastin or control cells. Fig. S3 shows verification of depletion of endogenous or exogenous spastin in the rescue experiments shown in Figs. 3 and 4. Fig. S4 demonstrates that CHMP1B depletion does not induce endosomal tubulation and that SNX1 and SNX4 colocalize on the tubules induced by IST1 depletion. Fig. S5 shows the endosomal tubules induced by spastin or IST1 depletion contain TfnR but not M6PR. Video 1 shows HeLa cells subjected to mock siRNA transfection and then transfected with SNX4-mCherry. Video 2 shows HeLa cells transfected with a pool of siRNA against spastin and then transfected with SNX4-mCherry. Video 3 shows HeLa cells transfected with a pool of siRNA against spastin and then transfected with SNX4-mCherry in which puncta and tubules can be seen to move together in several instances. Online supplemental material is available at http://www.jcb.org/cgi/content/full/jcb.201211045/DC1. Additional data are available in the JCB DataViewer at http://dx.doi.org/10.1083/jcb.201211045.dv.

We thank Susanne Bolte and the IFR83 imaging facility at Université Pierre et Marie Curie. We thank Matthew Gratian for advice on confocal microscopy experimental methodology.

E. Reid is a Wellcome Trust Senior Research Fellow in Clinical Science (grant no. 082381). M.N.J. Seaman is a UK Medical Research Council Senior Research Fellow (grant no. G0701444). The Cambridge Institute for Medical Research is supported by a Wellcome Trust Strategic Award (grant nos. 079895 and 100140). J. Hazan was supported by Association Strümpell-Lorrain and Association Française contre les Myopathies grants.

Submitted: 7 November 2012
Accepted: 19 June 2013

References

Agromayor, M., J.G. Carlton, J.P. Phelan, D.R. Matthews, L.M. Carlin, S. Ameer-Beg, K. Bowers, and J. Martin-Serrano. 2009. Essential role of hIST1 in cytokinesis. *Mol. Biol. Cell.* 20:1374–1387. http://dx.doi.org/10.1091/mbc.E08-05-0474

Babst, M., D.J. Katzmann, E.J. Estepa-Sabal, T. Meerloo, and S.D. Emr. 2002a. Escrt-III: an endosome-associated heterooligomeric protein complex required for mvb sorting. *Dev. Cell.* 3:271–282. http://dx.doi.org/10.1016/S1534-5807(02)00220-4

Babst, M., D.J. Katzmann, W.B. Snyder, B. Wendland, and S.D. Emr. 2002b. Endosome-associated complex, ESCRT-II, recruits transport machinery for protein sorting at the multivesicular body. *Dev. Cell.* 3:283–289. http://dx.doi.org/10.1016/S1534-5807(02)00219-8

Bajorek, M., E. Morita, J.J. Skalicky, S.G. Morham, M. Babst, and W.I. Sundquist. 2009a. Biochemical analyses of human IST1 and its function in cytokinesis. *Mol. Biol. Cell.* 20:1360–1373. http://dx.doi.org/10.1091/mbc.E08-05-0475

Bajorek, M., H.L. Schubert, J. McCullough, C. Langelier, D.M. Eckert, W.M. Stubblefield, N.T. Uter, D.G. Myszka, C.P. Hill, and W.I. Sundquist. 2009b. Structural basis for ESCRT-III protein autoinhibition. *Nat. Struct. Mol. Biol.* 16:754–762. http://dx.doi.org/10.1038/nsmb.1621

Blackstone, C., C.J. O'Kane, and E. Reid. 2011. Hereditary spastic paraplegias: membrane traffic and the motor pathway. *Nat. Rev. Neurosci.* 12:31–42. http://dx.doi.org/10.1038/nrn2990

Bonifacino, J.S., and J.H. Hurley. 2008. Retromer. *Curr. Opin. Cell Biol.* 20:427–436. http://dx.doi.org/10.1016/j.ceb.2008.03.009

Boucrot, E., A. Pick, G. Çamdere, N. Liska, E. Evergren, H.T. McMahon, and M.M. Kozlov. 2012. Membrane fission is promoted by insertion of amphipathic helices and is restricted by crescent BAR domains. *Cell.* 149:124–136. http://dx.doi.org/10.1016/j.cell.2012.01.047

Carlton, J. 2010. The ESCRT machinery: a cellular apparatus for sorting and scission. *Biochem. Soc. Trans.* 38:1397–1412. http://dx.doi.org/10.1042/BST0381397

Carlton, J., M. Bujny, B.J. Peter, V.M. Oorschot, A. Rutherford, H. Mellor, J. Klumperman, H.T. McMahon, and P.J. Cullen. 2004. Sorting nexin-1 mediates tubular endosome-to-TGN transport through coincidence sensing of high- curvature membranes and 3-phosphoinositides. *Curr. Biol.* 14:1791–1800. http://dx.doi.org/10.1016/j.cub.2004.09.077

Claudiani, P., E. Riano, A. Errico, G. Andolfi, and E.I. Rugarli. 2005. Spastin subcellular localization is regulated through usage of different translation start sites and active export from the nucleus. *Exp. Cell Res.* 309:358–369. http://dx.doi.org/10.1016/j.yexcr.2005.06.009

Connell, J.W., C. Lindon, J.P. Luzio, and E. Reid. 2009. Spastin couples microtubule severing to membrane traffic in completion of cytokinesis and secretion. *Traffic.* 10:42–56. http://dx.doi.org/10.1111/j.1600-0854.2008.00847.x

Derivery, E., C. Sousa, J.J. Gautier, B. Lombard, D. Loew, and A. Gautreau. 2009. The Arp2/3 activator WASH controls the fission of endosomes through a large multiprotein complex. *Dev. Cell.* 17:712–723. http://dx.doi.org/10.1016/j.devcel.2009.09.010

Egan, M.J., K. Tan, and S.L. Reck-Peterson. 2012. Lis1 is an initiation factor for dynein-driven organelle transport. *J. Cell Biol.* 197:971–982. http://dx.doi.org/10.1083/jcb.201112101

Fassier, C., J.A. Hutt, S. Scholpp, A. Lumsden, B. Giros, F. Nothias, S. Schneider-Maunoury, C. Houart, and J. Hazan. 2010. Zebrafish atlastin controls motility and spinal motor axon architecture via inhibition of the BMP pathway. *Nat. Neurosci.* 13:1380–1387. http://dx.doi.org/10.1038/nn.2662

Fassier, C., A. Tarrade, L. Peris, S. Courageot, P. Mailly, C. Dalard, S. Delga, N. Roblot, J. Lefèvre, D. Job, et al. 2013. Microtubule-targeting drugs rescue axonal swellings in cortical neurons from spastin knockout mice. *Dis. Model. Mech.* 6:72–83. http://dx.doi.org/10.1242/dmm.008946

Flanagan-Steet, H., M.A. Fox, D. Meyer, and J.R. Sanes. 2005. Neuromuscular synapses can form in vivo by incorporation of initially aneural postsynaptic specializations. *Development*. 132:4471–4481. http://dx.doi.org/10.1242/dev.02044

Frost, A., V.M. Unger, and P. De Camilli. 2009. The BAR domain superfamily: membrane-molding macromolecules. *Cell*. 137:191–196. http://dx.doi.org/10.1016/j.cell.2009.04.010

Gomez, T.S., and D.D. Billadeau. 2009. A FAM21-containing WASH complex regulates retromer-dependent sorting. *Dev. Cell*. 17:699–711. http://dx.doi.org/10.1016/j.devcel.2009.09.009

Guizetti, J., L. Schermelleh, J. Mäntler, S. Maar, I. Poser, H. Leonhardt, T. Müller-Reichert, and D.W. Gerlich. 2011. Cortical constriction during abscission involves helices of ESCRT-III-dependent filaments. *Science*. 331:1616–1620. http://dx.doi.org/10.1126/science.1201847

Hanson, P.I., S. Shim, and S.A. Merrill. 2009. Cell biology of the ESCRT machinery. *Curr. Opin. Cell Biol.* 21:568–574. http://dx.doi.org/10.1016/j.ceb.2009.06.002

Harbour, M.E., S.Y. Breusegem, R. Antrobus, C. Freeman, E. Reid, and M.N. Seaman. 2010. The cargo-selective retromer complex is a recruiting hub for protein complexes that regulate endosomal tubule dynamics. *J. Cell Sci.* 123:3703–3717. http://dx.doi.org/10.1242/jcs.071472

Hazan, J., N. Fonknechten, D. Mavel, C. Paternotte, D. Samson, F. Artiguenave, C.S. Davoine, C. Cruaud, A. Dürr, P. Wincker, et al. 1999. Spastin, a new AAA protein, is altered in the most frequent form of autosomal dominant spastic paraplegia. *Nat. Genet.* 23:296–303. http://dx.doi.org/10.1038/15472

Henne, W.M., N.J. Buchkovich, and S.D. Emr. 2011. The ESCRT pathway. *Dev. Cell*. 21:77–91. http://dx.doi.org/10.1016/j.devcel.2011.05.015

Henne, W.M., N.J. Buchkovich, Y. Zhao, and S.D. Emr. 2012. The endosomal sorting complex ESCRT-II mediates the assembly and architecture of ESCRT-III helices. *Cell*. 151:356–371. http://dx.doi.org/10.1016/j.cell.2012.08.039

Hu, J., Y. Shibata, P.P. Zhu, C. Voss, N. Rismanchi, W.A. Prinz, T.A. Rapoport, and C. Blackstone. 2009. A class of dynamin-like GTPases involved in the generation of the tubular ER network. *Cell*. 138:549–561. http://dx.doi.org/10.1016/j.cell.2009.05.025

Hurley, J.H. 2010. The ESCRT complexes. *Crit. Rev. Biochem. Mol. Biol.* 45:463–487. http://dx.doi.org/10.3109/10409238.2010.502516

Hurley, J.H., and D. Yang. 2008. MIT domainia. *Dev. Cell*. 14:6–8. http://dx.doi.org/10.1016/j.devcel.2007.12.013

Jones, C.B., E.M. Ott, J.M. Keener, M. Curtiss, V. Sandrin, and M. Babst. 2012. Regulation of membrane protein degradation by starvation-response pathways. *Traffic*. 13:468–482. http://dx.doi.org/10.1111/j.1600-0854.2011.01314.x

Kimmel, C.B., W.W. Ballard, S.R. Kimmel, B. Ullmann, and T.F. Schilling. 1995. Stages of embryonic development of the zebrafish. *Dev. Dyn.* 203:253–310. http://dx.doi.org/10.1002/aja.1002030302

Lauffer, B.E., C. Melero, P. Temkin, C. Lei, W. Hong, T. Kortemme, and M. von Zastrow. 2010. SNX27 mediates PDZ-directed sorting from endosomes to the plasma membrane. *J. Cell Biol.* 190:565–574. http://dx.doi.org/10.1083/jcb.201004060

Lenz, J.H., I. Schuchardt, A. Straube, and G. Steinberg. 2006. A dynein loading zone for retrograde endosome motility at microtubule plus-ends. *EMBO J.* 25:2275–2286. http://dx.doi.org/10.1038/sj.emboj.7601119

Lumb, J.H., J.W. Connell, R. Allison, and E. Reid. 2012. The AAA ATPase spastin links microtubule severing to membrane modelling. *Biochim. Biophys. Acta*. 1823:192–197. http://dx.doi.org/10.1016/j.bbamcr.2011.08.010

Maxfield, F.R., and T.E. McGraw. 2004. Endocytic recycling. *Nat. Rev. Mol. Cell Biol.* 5:121–132. http://dx.doi.org/10.1038/nrm1315

Montenegro, G., A.P. Rebelo, J. Connell, R. Allison, C. Babalini, M. D'Aloia, P. Montieri, R. Schüle, H. Ishiura, J. Price, et al. 2012. Mutations in the ER-shaping protein reticulon 2 cause the axon-degenerative disorder hereditary spastic paraplegia type 12. *J. Clin. Invest.* 122:538–544. http://dx.doi.org/10.1172/JCI60560

Motley, A., N.A. Bright, M.N. Seaman, and M.S. Robinson. 2003. Clathrin-mediated endocytosis in AP-2–depleted cells. *J. Cell Biol.* 162:909–918. http://dx.doi.org/10.1083/jcb.200305145

Nisar, S., E. Kelly, P.J. Cullen, and S.J. Mundell. 2010. Regulation of P2Y1 receptor traffic by sorting Nexin 1 is retromer independent. *Traffic*. 11:508–519. http://dx.doi.org/10.1111/j.1600-0854.2010.01035.x

Obita, T., S. Saksena, S. Ghazi-Tabatabai, D.J. Gill, O. Perisic, S.D. Emr, and R.L. Williams. 2007. Structural basis for selective recognition of ESCRT-III by the AAA ATPase Vps4. *Nature*. 449:735–739. http://dx.doi.org/10.1038/nature06171

Park, S.H., P.P. Zhu, R.L. Parker, and C. Blackstone. 2010. Hereditary spastic paraplegia proteins REEP1, spastin, and atlastin-1 coordinate microtubule interactions with the tubular ER network. *J. Clin. Invest.* 120:1097–1110. http://dx.doi.org/10.1172/JCI40979

Peden, A.A., E. Schonteich, J. Chun, J.R. Junutula, R.H. Scheller, and R. Prekeris. 2004. The RCP-Rab11 complex regulates endocytic protein sorting. *Mol. Biol. Cell*. 15:3530–3541. http://dx.doi.org/10.1091/mbc.E03-12-0918

Piper, R.C., and D.J. Katzmann. 2007. Biogenesis and function of multivesicular bodies. *Annu. Rev. Cell Dev. Biol.* 23:519–547. http://dx.doi.org/10.1146/annurev.cellbio.23.090506.123319

Reaves, B.J., N.A. Bright, B.M. Mullock, and J.P. Luzio. 1996. The effect of wortmannin on the localisation of lysosomal type I integral membrane glycoproteins suggests a role for phosphoinositide 3-kinase activity in regulating membrane traffic late in the endocytic pathway. *J. Cell Sci.* 109:749–762.

Reid, E., J. Connell, T.L. Edwards, S. Duley, S.E. Brown, and C.M. Sanderson. 2005. The hereditary spastic paraplegia protein spastin interacts with the ESCRT-III complex-associated endosomal protein CHMP1B. *Hum. Mol. Genet.* 14:19–38. http://dx.doi.org/10.1093/hmg/ddi003

Renvoisé, B., R.L. Parker, D. Yang, J.C. Bakowska, J.H. Hurley, and C. Blackstone. 2010. SPG20 protein spartin is recruited to midbodies by ESCRT-III protein Ist1 and participates in cytokinesis. *Mol. Biol. Cell*. 21:3293–3303. http://dx.doi.org/10.1091/mbc.E09-10-0879

Riano, E., M. Martignoni, G. Mancuso, D. Cartelli, F. Crippa, I. Toldo, G. Siciliano, D. Di Bella, F. Taroni, M.T. Bassi, et al. 2009. Pleiotropic effects of spastin on neurite growth depending on expression levels. *J. Neurochem.* 108:1277–1288. http://dx.doi.org/10.1111/j.1471-4159.2009.05875.x

Roll-Mecak, A., and R.D. Vale. 2008. Structural basis of microtubule severing by the hereditary spastic paraplegia protein spastin. *Nature*. 451:363–367. http://dx.doi.org/10.1038/nature06482

Sanderson, C.M., J.W. Connell, T.L. Edwards, N.A. Bright, S. Duley, A. Thompson, J.P. Luzio, and E. Reid. 2006. Spastin and atlastin, two proteins mutated in autosomal-dominant hereditary spastic paraplegia, are binding partners. *Hum. Mol. Genet.* 15:307–318. http://dx.doi.org/10.1093/hmg/ddi447

Seaman, M.N. 2004. Cargo-selective endosomal sorting for retrieval to the Golgi requires retromer. *J. Cell Biol.* 165:111–122. http://dx.doi.org/10.1083/jcb.200312034

Shim, S., L.A. Kimpler, and P.I. Hanson. 2007. Structure/function analysis of four core ESCRT-III proteins reveals common regulatory role for extreme C-terminaldomain.*Traffic*.8:1068–1079.http://dx.doi.org/10.1111/j.1600-0854.2007.00584.x

Splinter, D., D.S. Razafsky, M.A. Schlager, A. Serra-Marques, I. Grigoriev, J. Demmers, N. Keijzer, K. Jiang, I. Poser, A.A. Hyman, et al. 2012. BICD2, dynactin, and LIS1 cooperate in regulating dynein recruitment to cellular structures. *Mol. Biol. Cell*. 23:4226–4241. http://dx.doi.org/10.1091/mbc.E12-03-0210

Stuchell-Brereton, M.D., J.J. Skalicky, C. Kieffer, M.A. Karren, S. Ghaffarian, and W.I. Sundquist. 2007. ESCRT-III recognition by VPS4 ATPases. *Nature*. 449:740–744. http://dx.doi.org/10.1038/nature06172

Temkin, P., B. Lauffer, S. Jäger, P. Cimermancic, N.J. Krogan, and M. von Zastrow. 2011. SNX27 mediates retromer tubule entry and endosome-to-plasma membrane trafficking of signalling receptors. *Nat. Cell Biol.* 13:715–721. http://dx.doi.org/10.1038/ncb2252

Traer, C.J., A.C. Rutherford, K.J. Palmer, T. Wassmer, J. Oakley, N. Attar, J.G. Carlton, J. Kremerskothen, D.J. Stephens, and P.J. Cullen. 2007. SNX4 coordinates endosomal sorting of TfnR with dynein-mediated transport into the endocytic recycling compartment. *Nat. Cell Biol.* 9:1370–1380. http://dx.doi.org/10.1038/ncb1656

Tsang, H.T., T.L. Edwards, X. Wang, J.W. Connell, R.J. Davies, H.J. Durrington, C.J. O'Kane, J.P. Luzio, and E. Reid. 2009. The hereditary spastic paraplegia proteins NIPA1, spastin and spartin are inhibitors of mammalian BMP signalling. *Hum. Mol. Genet.* 18:3805–3821. http://dx.doi.org/10.1093/hmg/ddp324

van Weering, J.R.T., P. Verkade, and P.J. Cullen. 2012. SNX-BAR-mediated endosome tubulation is co-ordinated with endosome maturation. *Traffic*. 13:94–107. http://dx.doi.org/10.1111/j.1600-0854.2011.01297.x

Wang, X., W.R. Shaw, H.T. Tsang, E. Reid, and C.J. O'Kane. 2007. *Drosophila* spichthyin inhibits BMP signaling and regulates synaptic growth and

axonal microtubules. *Nat. Neurosci.* 10:177–185. http://dx.doi.org/10.1038/nn1841

Wassmer, T., N. Attar, M. Harterink, J.R. van Weering, C.J. Traer, J. Oakley, B. Goud, D.J. Stephens, P. Verkade, H.C. Korswagen, and P.J. Cullen. 2009. The retromer coat complex coordinates endosomal sorting and dynein-mediated transport, with carrier recognition by the trans-Golgi network. *Dev. Cell*. 17:110–122. http://dx.doi.org/10.1016/j.devcel.2009.04.016

Wollert, T., C. Wunder, J. Lippincott-Schwartz, and J.H. Hurley. 2009. Membrane scission by the ESCRT-III complex. *Nature*. 458:172–177. http://dx.doi.org/10.1038/nature07836

Wood, J.D., J.A. Landers, M. Bingley, C.J. McDermott, V. Thomas-McArthur, L.J. Gleadall, P.J. Shaw, and V.T. Cunliffe. 2006. The microtubule-severing protein Spastin is essential for axon outgrowth in the zebrafish embryo. *Hum. Mol. Genet.* 15:2763–2771. http://dx.doi.org/10.1093/hmg/ddl212

Yang, D., N. Rismanchi, B. Renvoisé, J. Lippincott-Schwartz, C. Blackstone, and J.H. Hurley. 2008. Structural basis for midbody targeting of spastin by the ESCRT-III protein CHMP1B. *Nat. Struct. Mol. Biol.* 15:1278–1286. http://dx.doi.org/10.1038/nsmb.1512

Zamborlini, A., Y. Usami, S.R. Radoshitzky, E. Popova, G. Palu, and H. Göttlinger. 2006. Release of autoinhibition converts ESCRT-III components into potent inhibitors of HIV-1 budding. *Proc. Natl. Acad. Sci. USA*. 103:19140–19145. http://dx.doi.org/10.1073/pnas.0603788103